haematologica
Journal of the Ferrata Storti Foundation

HES1 regulates bone marrow mesenchymal stromal cell function by suppressing NFATc2-mediated inflammation

by Anthony Z. Zhu, Zhilin Ma, Emily V. Wolff, Sanghoon Lee, Zichen L. Lin, Zhenxia J. Gao and Wei Du

Received: May 15, 2025.
Accepted: September 24, 2025.

Citation: Anthony Z. Zhu, Zhilin Ma, Emily V. Wolff, Sanghoon Lee, Zichen L. Lin, Zhenxia J. Gao and Wei Du. HES1 regulates bone marrow mesenchymal stromal cell function by suppressing NFATc2-mediated inflammation.
Haematologica. 2025 Oct 2. doi: 10.3324/haematol.2025.288138 [Epub ahead of print]

HES1 regulates bone marrow mesenchymal stromal cell function by suppressing NFATc2-mediated inflammation

Anthony Z. Zhu[1, 2, *], Zhilin Ma[3, *], Emily V. Wolff[1, 2, 4 *], Sanghoon Lee[1, 2], Zichen Lin[5], Zhenxia J. Gao[1, 2], Wei Du[1, 2]

[1]Division of Oncology, University of Pittsburgh School of Medicine, Pittsburgh, PA; [2]UPMC Hillman Cancer Center, Pittsburgh, PA; [3]Department of Biological Sciences, University of Notre Dame, Notre Dame, IN; [4]Graduate Program, Pennsylvania State University School of Medicine, Hershey, PA; [5]Master of Science in Medical Science, Boston University School of Medicine Graduate Master Program, Boston, MA

Address correspondence to: Wei Du, Division of Hematology and Oncology, University of Pittsburgh School of Medicine; UPMC Hillman Cancer Center, 5117 Center Ave, Pittsburgh, PA 15213. Email: wed41@pitt.edu

*: contribute equally to the work

Running title: HES1 regulates MSC function

Key word: HES1, Mesenchymal stromal cells, Hematopoiesis, inflammation

AUTHOR CONTRIBUTIONS

A.Z.Z., Z.M. and E.V.W., performed the research, analyzed the data; Z.L., and Z.G. performed some of the research, assisted data analysis; S.L. performed bioinformatics

analysis; W.D. designed the research, analyzed the data, wrote the paper.

Conflicts of interest

The authors declare no conflicts of interest.

Data availability statement

The raw RNA-seq data are available through the Gene Expression Omnibus (GEO) database under the accession number GSE296738. The data that support the findings of this study are available from the corresponding author upon reasonable request.

Acknowledgments

We thank Dr. Ryoichiro Kageyama (Kyoto University) for *Hes1*$^{fl/fl}$ mice, and Asher Y. Peng for assisting mouse genotyping. This work is supported by NIH/National Heart, Lung, and Blood Institute grants (R01HL151390 and R56HL169348 to W.D.), a NIH/National Cancer Institute grant (R01CA285400 to W.D.), and a NIH/National Institute of Aging grant (R01AG093995 to W.D.). This project used the Hillman Animal Facility, supported in part, by NIH/NCI grant P30CA047904. W.D. is supported by a Leukemia and Lymphoma Society (LLS) Scholar Award.

Conflicts of interest

The authors declare no conflicts of interest.

Ethical approval and consent to participate

No human data is used. Title of the approved project: “Role of FA proteins in hematopoiesis”. Name of the institutional approval committee or unit: Institutional Animal Care and Use Committee, University of Pittsburgh (Approval number: 24044702)

Abstract

The Notch target gene, Hairy and enhancer of split-1 (HES1), encodes a basic helix-loop-helix transcriptional repressor that influences cell proliferation and differentiation in embryogenesis. Our previous studies indicate that HES1 is required for hematopoiesis under stress conditions. However, the role of HES1 in bone marrow (BM) microenvironment remains elucidated. By employing a BM niche specific *Hes1* knockout mouse model, here we have investigated the role of HES1 in regulating mesenchymal stromal cell (MSC) homeostasis and their hematopoiesis supportive function. We found that while HES1 is dispensable in MSC in supporting steady-state hematopoiesis, *Hes1*$^{fl/fl}$*Prx1Cre* mice are hypersensitive to lipopolysaccharide (LPS) challenge. Deletion of *Hes1* in the BM reduces MSC frequency and affects MSC self-renewal and proliferation. *Hes1*-deficient MSCs are less functional in supporting hematopoiesis both *in vitro* and *ex vivo*. Transcriptome analysis reveals that disruption of *Hes1* in the BM stroma alters the expression of genes critical for cellular metabolism and inflammation. Pharmacological blockage of inflammation rescues *Hes1*-KO MSC phenotype and improves their hematopoiesis supportive function. Mechanistically, we show that HES1 binds to the conserved E boxes in the promoter of NFATc2, a member of the AT-rich interaction domain superfamily of DNA binding protein, to suppress NFATc2-mediated inflammation. Taken together, our study unveils a pivotal role of HES1 in maintaining BM MSC hemostasis and regulating their hematopoiesis supportive function.

Introduction

Hematopoietic stem cells (HSCs), which give rise to all blood cells, are supported by specialized microenvironments, known as niches, within bone marrow (BM) cavities (1, 2). These niches comprise of various nonhematopoietic components, including endosteal and sinusoidal endothelial cells, mesenchymal stromal cells (MSCs), and osteoblast-lineage cells (3, 4). Studies have shown that BM-derived non-hematopoietic stromal cells are capable of supporting long-term hematopoiesis both *in vitro* and *in vivo*. Disruptions to these non-hematopoietic cells within the BM niche may negatively impact hematopoiesis. However, the precise mechanism is still poorly understood.

Notch signaling, mediated by a family of highly conserved receptors, plays a critical role in maintaining bone homeostasis, partly through regulating osteoblast differentiation from MSCs, whose activation is induced by their specific ligands (5, 6). One key Notch target, HES1, a mammalian counterpart of the Hairy and Enhancer of split proteins, is essential in various physiological processes including cellular differentiation, cell cycle arrest, apoptosis and self-renewal ability (7). HES1 has been shown to inhibit adipogenesis in porcine mesenchymal stem cells by repressing FAD24 transcription (8). In mice, deletion of *Hes1* causes severe neural tube defects and defects in other organs, such as the thymus, pancreas, gut, bile duct, and neutral tube leading to lethality during late embryogenesis (9, 10). Our previous work demonstrated that HES1 prevents replication-induced HSC exhaustion by suppressing fatty acid oxidation (FAO; 11). However, the role of HES1 in the BM microenvironment remains underexplored.

Signals from the BM niche are crucial in regulating blood production. For instance, inflammation within the stromal niche, driven by IL-1 signaling, has been implicated in hematopoietic aging (12). During infection or systemic inflammation, HSCs respond to inflammatory stimuli, such as pathogen-derived signals and cytokines, through a process termed as emergency myelopoiesis, which includes HSC activation, expansion and enhanced myeloid differentiation. Niche cell populations contribute to this process by secreting paracrine factors in response to pro-inflammatory signals, thereby indirectly influencing HSC function (13). Numerous studies have shown (14) a correlation between elevated circulating pro-inflammatory cytokines and anemia in patients with leukemia-related BM diseases, such as Fanconi anemia (FA), a genetic disorder associated with BM failure and leukemia. However, direct evidence linking niche-related inflammation to HSC maintenance is still lacking.

NFATc2 (Nuclear factor of activated T- cells, cytoplasmic 2), is a member of the NFAT gene family that regulates various biological processes, including immune responses, inflammation, angiogenesis, bone homeostasis, and cancer development and metastasis (15). NFATc2 is activated by signals, such as calcium influx, and regulates the transcription of genes associated with inflammation and immune cell activation. In immune cells such as T cells, NFATc2 activation promotes cytokine production during both acute and chronic inflammatory responses (16). NFATc2 is also implicated in autoimmune diseases and other inflammatory disorders due to its regulation of immune cell activity (17). Beyond immune cells, NFATc2 influences endothelial cell activation and other tissues involved in inflammation (18). NFATc2 has been shown to play a role in regulating the BM niche, particularly in modulating the

behavior of hematopoietic stem and progenitor cells (HSPCs). It contributes to the activation of signaling pathways within the BM niche, affecting stem cell self-renewal, differentiation, and migration (19). In mice, *NFATc2* deficiency in HSPCs leads to severe hematological abnormalities (20). However, the indirect role of NFATc2 in BM-derived MSCs is largely unknown.

In the present study, we investigate the role of HES1 in the BM microenvironment using a mouse model carrying mesenchymal specific *Hes1* deletion. We found that loss of *Hes1* leads defects in MSC self-renewal, compromising their ability to support hematopoiesis and promoting increased mesenchymal inflammation. Mechanistically, we demonstrate that HES1 binds to E-boxes within the NFATc2 promoter to suppress NFATc2-mediated inflammation, thereby regulating the hematopoiesis supportive function of BM MSCs. Our findings underscore a critical role of HES1 in maintaining MSC homeostasis and function.

Methods

Mice and treatment

Heterozygous *Hes1*$^{fl/+}$ mice in a C57BL/6 background (11, 21) were generated from the sperm purchased at Experimental Animal Division at RIKEN Bioresource Center (RBRC #: RBRC06047). Heterozygous *Hes1*$^{fl/+}$ mice were interbred with *Prx1Cre* (Prrx1^{Cre}) mice to generate MSC specific *Hes1* deletion (22, 23). *Prx1Cre* transgenic mice have the Prx1 promoter/enhancer directing Cre recombinase expression to early limb bud mesenchyme and a subset of craniofacial mesenchyme. The mice were backcrossed more than 10 times before the experiments listed below.

6~8-week-old BoyJ mice were used as bone marrow transplant (BMT) recipients. Animals including BoyJ recipient mice were maintained in the animal barrier facility at the University of Pittsburgh. All experimental procedures conducted in this study were approved by the Institutional Animal Care and Use Committee of University of Pittsburgh.

Mesenchymal stromal cell (MSC) culture and treatment

Whole bone marrow cells (WBMCs) from *Hes1*$^{fl/fl}$*Prx1Cre* or *Hes1*$^{fl/fl}$ mice were gently flushed out of tibias and femurs using DPBS + 10% FBS. Cells obtained from two tibias and two femurs were plated in 100mm culture dish (BD Falcon, Tewksbury, MA) in 10 ml of MSCs media (Mouse MesenCult Basal Medium supplemented with MesenCult Supplement; Stem Cell Technologies) adapted and modified from previous reports (24).

For the blockade experiments, MSCs were *ex vivo* cultured in the presence of different inhibitors, such as TNF-α neutralization antibody (R&D Systems; 25), CXCR2 antagonist (AZD5069; Medchem Express; 26), IL-1R antagonist (AF12198, MedChem

Express; 27), CCR3 antagonist (GW76694, Medchem Express; 28), followed by *in vitro* or *in vivo* functional analysis. NFATc2 inhibitor, 11R-VIVIT (29) was purchased from MedChem Express.

Bone marrow transplantation (BMT)

Progenies of WT SLAM ($Lin^-Sca1^+c\text{-}kit^+CD150^+CD48^-$) cells ($CD45.2^+$) co-cultured with MSCs from *Hes1*$^{fl/fl}$*Prx1Cre* mice or their *Hes1*$^{fl/fl}$ littermates were transplanted into lethally irradiated BoyJ recipients ($CD45.1^+$). Donor-derived chimera ($CD45.1^+$) were analyzed at different time points post BMT.

For reverse BMT, 1 million WBMCs BoyJ mice ($CD45.1^+$) were injected into lethally irradiated *Hes1*$^{fl/fl}$*Prx1Cre* mice or their *Hes1*$^{fl/fl}$ littermates ($CD45.2^+$). After 16 weeks, the recipient mice were sacrificed, and nucleated cells from peripheral blood (PB) and the BM were analyzed were stained with CD45.2 and CD45.1 for donor-derived chimeras. For secondary BMT, 3 million WBMCs from primary recipients were pooled and injected into sublethally irradiated (7.0 Gy) *Hes1*$^{fl/fl}$*Prx1Cre* mice or their *Hes1*$^{fl/fl}$ littermates.

For lineage differentiation, single-cell suspensions were incubated with various combination of the following cell surface marker antibodies: CD45.1-FITC, Gr1-APC, Mac1-PE-Cy7, CD45.2-APC, CD3ε (all from BD PharMingen) and B220-PE (eBiosceinces, Cat # 12-0452-85). Immunolabeled cells were analyzed by flow cytometry.

For BMT using progenies from the co-culture, $1X10^5$ output cells ($CD45.2^+$) collected from cocultures were mixed with $3X10^5$ competitor cells ($CD45.1^+$), and

injected into lethally irradiated BoyJ mice (CD45.1^{+}). After 16 weeks, the recipient mice were sacrificed, and nucleated cells from PB and the BM were analyzed by staining with CD45.2 and CD45.1 for donor-derived chimeras. For secondary BMT, 3 million WBMCs from primary recipients were pooled and injected into sublethally irradiated (7.0 Gy) BoyJ recipients.

Results

Mesenchymal *Hes1* is dispensable for steady state hematopoiesis

To elucidate the role of HES1 in the bone marrow (BM) microenvironment, we recently generated a mouse model with constitutive deletion of *Hes1* specifically in mesenchymal stromal lineages (*Hes1*$^{fl/fl}$*Prx1Cre*), by crossing a previously established conditional *Hes1* knockout strain (*Hes1*$^{fl/fl}$; 11, 21) with mesenchymal-specific *Prx1Cre* deleters. Expression of Cre recombinase under the promoter of Prx1, induces deletion of *Hes1* alleles, specifically in mesenchymal lineages (22, 23). The genotypes of offspring followed Mendelian frequencies, indicating that no embryonic lethality or perinatal lethality was associated with the BM microenvironment *Hes1* deletion (Fig S1A). qPCR analysis and flow-based intracellular Hes1 staining using MSCs from *Hes1*$^{fl/fl}$*Prx1Cre* mice confirmed a successful deletion of *Hes1* in mouse BM niche (Fig S1B, S1C).

We first examined the effect of *Hes1* deletion on steady state hematopoiesis by monitoring the peripheral blood (PB) parameters in 6 to 8-week-old mice using HemaVet 950. We noticed a slight increase in white blood cell (WBC) counts in *Hes1*$^{fl/fl}$*Prx1Cre* mice than *Hes1*$^{fl/fl}$ control animals. However, there was no significant

difference in the hemoglobin and hematocrit values between *Hes1*$^{fl/fl}$*Prx1Cre* mice and their *Hes1*$^{fl/fl}$ littermates (Table S1). All other hematological parameters, including total erythrocyte counts, appeared to be normal in *Hes1*$^{fl/fl}$*Prx1Cre* mice, as compared to their *Hes1*$^{fl/fl}$ littermates. Therefore, there is no indication of anemia in these mutant animals under a steady state.

We then examined the BM of *Hes1*$^{fl/fl}$*Prx1Cre* mice and observed a comparable total BM cellularity of *Hes1*$^{fl/fl}$*Prx1Cre* mice in comparison to their *Hes1*$^{fl/fl}$ littermates (Fig 1A). Further analysis of the mice showed no effect of *Hes1* deletion on the relative frequencies of hematopoietic progenitor cells (LSK; Lin$^-$Sca1$^+$c-kit$^+$) and the phenotypic HSCs (Lin$^-$Sca1$^+$c-kit$^+$CD150$^+$CD48$^-$; Signaling lymphocyte activation molecules, SLAM) compartment (Fig 1B), suggesting that mesenchymal deletion of *Hes1* does not alter BM hematopoietic stem progenitor cell (HSPC) composition.

Quiescence is a critical feature of HSC homeostasis (30). We next analyzed the cell cycle profile of HSCs from *Hes1*$^{fl/fl}$*Prx1Cre* mice. Ki67/DAPI staining revealed a slight decrease, albeit not statistically significant, in the proportion of quiescent (G0) and a slight increase in the proportion of cycling (S/G2/M) SLAM cells in *Hes1*$^{fl/fl}$*Prx1Cre* mice compared to *Hes1*$^{fl/fl}$ control animals (Fig1C). Moreover, loss of *Hes1* did not affect the viability of SLAM cells at the steady state (Fig 1D). These results suggest that the mesenchymal HES1 is dispensable for steady-state hematopoiesis.

Hes1$^{fl/fl}$*Prx1Cre* mice are hypersensitive to LPS challenge

We then examined immune response in mice deficient for *Hes1* in BM niche and found that *Hes1*$^{fl/fl}$*Prx1Cre* mice were highly susceptible to septic shock (Fig 2A) induced by lipopolysaccharide (LPS), an immunological endotoxin from Gram-negative bacteria and

can cause an acute inflammatory response by triggering the release of a vast number of inflammatory cytokines in various cell types (31). LPS treatment in *Hes1*$^{fl/fl}$*Prx1Cre* mice resulted in cytopenia, as evidenced by reduced red blood cell (RBC) counts, hemoglobin levels, and hematocrit values (Fig 2B). Additionally, BM analysis of LPS-treated *Hes1*$^{fl/fl}$*Prx1Cre* mice showed a significant decrease in BM cellularity (Fig 2C). In a separate set of experiments assessing hematopoietic recovery after LPS injection, we observed that *Hes1*$^{fl/fl}$*Prx1Cre* mice took significantly longer to recover from hematopoietic suppression (Fig 2D), requiring up to twice the time of wild-type (WT) mice to return to pre-treatment levels (Fig 2B). We also observed sustained low counts of white blood cells (WBCs), neutrophils (NEU) and lymphocytes (Lymph) in *Hes1*$^{fl/fl}$*Prx1Cre* mice after LPS injection (Fig 2E). These findings suggest that mesenchymal HES1 plays a critical role in the maintenance of hematopoietic stem cells (HSCs) under inflammatory stress.

It is known that myeloid ablation agent Fluorouracil (5-FU) induces hyper-proliferation and exhaustion of HSCs. To strengthen the physiological relevance of these findings, we then administered *Hes1*$^{fl/fl}$*Prx1Cre* mice with 5-FU, and found a similar drop of WBC count at the first week after 5-FU injection in both *Hes1*$^{fl/fl}$ and *Hes1*$^{fl/fl}$*Prx1Cre* mice (Fig S2A). However, WBC recovery in *Hes1*$^{fl/fl}$ mice started as early as 10 days after 5-FU treatment, whereas the recovery of WBC count in *Hes1*$^{fl/fl}$*Prx1Cre* mice persistently lagged as compared to *Hes1*$^{fl/fl}$ mice (Fig S2A). Consequently, 5-FU caused significantly increased mortality of *Hes1*$^{fl/fl}$*Prx1Cre* mice compared to control animals (Fig S2B). Thus, inactivation of Hes1 in the BM niche renders mice hypersensitive to 5-FU-induced BM ablation.

Hes1 deletion in BM niche affects MSC self-renewal

Since *Hes1*$^{fl/fl}$*Prx1Cre* mice are only defective for *Hes1* in mesenchymal compartment, to examine whether *Hes1* deletion directly alters the BM stromal cell composition *in vivo*, we performed flow cytometry analysis on whole bone marrow cells (WBMCs) stained with a panel of antibodies including CD45, CD44, CD105, CD73, CD146, and CD90 (32). A slight reduction in the $CD45^{-}CD44^{+}CD105^{+}CD73^{+}CD146^{+}CD90^{+}$ BM MSC population was observed in the BM of *Hes1*$^{fl/fl}$*Prx1Cre* mice compared with *Hes1*$^{fl/fl}$ littermates (Fig 3A). Consistently, colony-forming-unit fibroblast (CFU-F) assay (33), a well-established method to determine BM MSC frequency *in vivo*, using freshly isolated WBMCs (passage 0), revealed a significantly reduced frequency of CFU-F in *Hes1*$^{fl/fl}$*Prx1Cre* BM compared with *Hes1*$^{fl/fl}$ controls (Fig 3B, Left). In addition, the size of the colonies formed by *Hes1*-KO MSCs were also smaller than those formed by control MSCs. Notably, fewer colonies were formed by *Hes1*$^{fl/fl}$*Prx1Cre* MSCs compared with control MSCs (Fig 3B, Right). Additionally, MSCs from *Hes1*$^{fl/fl}$*Prx1Cre* mice showed increased quiescence (Fig S3A) and are less proliferative (Fig S3B), consistent with our previous study that *Hes1* loss in fetal hematopoietic compartment affects cell quiescence (21). These results indicate that *Hes1* deletion in the BM niche decreases the BM MSC pool and their CFU-F capacity *in vivo*.

As a major component of BM niche, MSCs serve as precursors to osteoblasts, and adipocytes, playing a crucial role in maintaining HSC quiescence (34). To further assess the impact of *Hes1* loss on MSC differentiation, we performed CFU-osteoblast and CFU-adipocyte differentiation assays (33, 35), using primary BM mononuclear cells from *Hes1*$^{fl/fl}$ and *Hes1*$^{fl/fl}$*Prx1Cre* mice. Differentiation of BM MSCs in lipid culture

conditions showed that *Hes1*$^{fl/fl}$*Prx1Cre* BM-derived MSCs gave rise to similar numbers of ALP^{+} osteoblastic colonies (Fig 3C) and Oil Red O^{+} colonies (Fig 3D). Collectively, these results suggest that loss of *Hes1* impairs BM MSC self-renewal and proliferation but has a minimal effect on MSC differentiation. This finding further supports the notion that the observed LPS hypersensitivity (Fig 2) is not due to increased lipid accumulation in BM, which is consistent with our earlier observations (Fig 1).

Loss of *Hes1* compromises hematopoiesis supportive function of MSCs

The BM niche provides the essential environment for HSCs (35). To characterize the hematopoiesis-supportive function of MSCs deficient for *Hes1*, we conducted *ex vivo* Cobblestone formation assay (24), by co-culturing wild-type (WT) LSK cells (Lin^{-}Sca1^{+}c-kit^{+}; enriched for HSPCs) with *Hes1*$^{fl/fl}$*Prx1Cre* or *Hes1*$^{fl/fl}$ MSCs in MSC culture medium (Fig 4A; 24, 33). Our results revealed that the cobblestone areas formed by WT cells co-cultured on *Hes1-KO* MSCs were significantly smaller than those co-cultured with control MSCs (Fig 4B).

Functionally, WT progenies co-cultured with *Hes1-KO* MSCs exhibited compromised progenitor activity as shown by CFU assay (Fig 4C), and reduced capacity to reconstitute donor-derived hematopoiesis (CD45.2^{+}) in the lethally irradiated BoyJ recipients (CD45.1^{+}; Fig 4D). In addition, the progenies from *Hes1*-KO MSC co-culture showed significantly diminished long-term reconstitution in secondary transplanted recipients (Fig 4E). Moreover, donor-derived LSK, SLAM cells in the recipients transplanted with progenies co-cultured with *Hes1*-KO MSCs were substantially lower than those transplanted with progenies from control MSCs co-culture

(Fig 4F), suggesting that deletion of *Hes1* compromised hematopoiesis-supportive function of MSCs *in vitro*.

To further validate our findings, we performed reverse BMT by injecting WBMCs from BoyJ mice (WT; CD45.1^{+}) into lethally irradiated *Hes1*$^{fl/fl}$*Prx1Cre* or *Hes1*$^{fl/fl}$ control mice (CD45.2^{+}; Fig 4G). Flow cytometry analysis at different time points post BMT, showed significantly reduced donor-derived chimera (CD45.1^{+}) in *Hes1*$^{fl/fl}$*Prx1Cre* recipients compared to those in *Hes1*$^{fl/fl}$ recipients, further confirming the compromised hematopoiesis supportive function of *Hes1*-KO MSCs *in vivo* (Fig 4H). Additionally, there was a myeloid-biased lineage differentiation in *Hes1*$^{fl/fl}$*Prx1Cre* recipients compared to *Hes1*$^{fl/fl}$ recipients (Fig S4).

These findings were further supported by the observation that HSPCs from naïve *Hes1*$^{fl/fl}$*Prx1Cre* mice were less functional in generating colonies in colony forming unit (CFU) assay (Fig S5A) and exhibited defects in reconstituting hematopoiesis in irradiated primary (Fig S5B) and secondary recipients (Fig S5C). Taken together, these data highlight the essential role of HES1 in regulating hematopoiesis supportive function of MSC.

Hes1 deficiency alters transcriptomic profile in MSCs

To explore the underlying mechanisms, we performed RNA-seq analysis using sorted BM MSCs (24) from *Hes1*$^{fl/fl}$*Prx1Cre* or *Hes1*$^{fl/fl}$ control mice. We observed approximately 800 differentially expressed genes in *Hes1*$^{fl/fl}$*Prx1Cre* MSCs compared to *Hes1*$^{fl/fl}$ MSCs (Fig 5A). Gene set enrichment analysis (GSEA) indicated that the dysregulated genes were significantly enriched in pathways related to cellular

metabolism, including Oxidative Phosphorylation (OXPHOS), Glycolysis, Fatty acid metabolism (Fig 5B), consistent with previous observations (11, 36). Notably, multiple inflammation-related pathways were upregulated in *Hes1*-KO MSCs, including interferon alpha response, IL6_JAK_STAT3 signaling, inflammatory response, and p53 pathway (Fig 5B, 5C).

Given the significant alterations observed in inflammation-related genes, we next performed master regulator analysis (MRA), a widely used method to identify transcriptional perturbations from gene expression profiles (37) and identified a set of transcription factors (TFs) associated with heightened inflammation in *Hes1*-defiecient MSCs (Fig 5D). These results indicate that loss of HES1 alters transcriptional programs in MSCs.

Pharmacological inhibition of excessive niche inflammation rescues MSC phenotype

Since we observed substantial expression changes in genes and pathways involved in inflammation, to test if stromal inflammation is a key factor contributing to MSC defects observed in *Hes1*$^{fl/fl}$*Prx1Cre* mice, we performed CellPhoneDB analysis, an established tool to detect a repository of ligands, receptors and their interactions (38) and find the gene pair of ligand-receptor expressed in *Hes1*-KO in comparison to control MSCs. The results showed a significant set of alterations in ligand-receptor interactions in *Hes1*-KO MSCs compared to the control MSCs (Fig S6A). Among the significantly upregulated inflammatory genes, we observed that several TNF-α, IL-1R, CXCR2-related ligand-receptor pairs were significantly upregulated in *Hes1*-KO MSCs (Fig S6). Indeed, mRNA

levels of inflammatory genes, including *Tnfa, Cxcl4, Il1b* and *Ccl11* were significantly elevated in *Hes1*-KO MSCs compared to those in control MSCs (Fig S7).

Previous studies have shown that inflammation-induced TNF-α eliminates myeloid progenitors, while preventing necroptosis of HSCs and initiating emergency myelopoiesis through NF-κB-dependent mechanisms, thus promoting HSC survival and hematopoietic regeneration (39). CXCR2 and its ligand CXCL4 have critical roles in regulating the survival and self-renewal of HSPCs (40) through modulating neutrophil mobilization (41). The endogenous IL-1 receptor antagonist limits healthy and malignant myeloproliferation (42). Furthermore, CCL11-CCR3 interaction has been implicated in promoting lymphoma cell survival (43). To explore the functional relevance of these HES1-inflammation signatures in the *Hes1*-KO MSCs, we conducted blockade experiments using the neutralizing antibody against TNF-α (25), the CXCR2 antagonist, AZD5069 (26), the IL-1R antagonist, AF12198 (27) or CCR3 antagonist GW76694 (28). The results demonstrated that inhibition of inflammation rescued colony formation ability of *Hes1*-KO MSC (Fig 6A) and cobblestone areas formed by inflammation inhibitor treated *Hes1*-KO MSCs were significantly larger compared to those treated with vehicle (Fig 6B). Functionally, the progenies from *Hes1*-KO MSC co-culture in the presence of inflammatory inhibitors, produced remarkably more colonies in CFU assay (Fig 6C) and established significantly higher donor-derived chimera in the transplanted recipients (Fig 6D), compared to those treated with vehicle only. Furthermore, systemic injection of inflammatory inhibitors to the recipient mice transplanted with WT progenies co-cultured with *Hes1*$^{fl/fl}$*Prx1Cre* MSCs also rescues the defects *in vivo* (Fig 6E). Together, these

data indicate that HES1 regulates hematopoiesis supportive function of BM MSCs, potentially through the suppression of inflammation.

HES1 binds to E boxes in NFATc2 promoter to suppress downstream inflammatory gene expression in MSCs

Our MRA analysis identified several potential transcription factors (TFs) downstream of HES1 in suppressing inflammation in mouse MSCs (Fig 5C). Among these, NFATc2 particularly caught our attention due to its potential role in modulating inflammation (16-18). We first confirmed the increased expression of *Nfatc2* in *Hes1*-KO MSCs compared to those in *Hes1*$^{fl/fl}$ control MSCs by quantitative PCR analysis (qPCR; Fig S8).

To assess whether NFATc2 directly regulates inflammatory gene expression in MSCs, we treated MSCs isolated from *Hes1*$^{fl/fl}$*Prx1Cre* mice or *Hes1*$^{fl/fl}$ mice with NFATc2 inhibitor, 11R-VIVIT (29) and found that inhibition of NFATc2 significantly reduced the levels of inflammatory cytokines in the MSC culture medium (Fig 7A). These results suggest that NFATc2 might serve as a downstream factor of HES1 in repressing inflammatory gene expression in the BM-derived MSCs. To test the notion, we measured the activity of NFATc2 promoter using a previously described 1.5 kb NFATc2 promoter-luciferase reporter (44), in response to ectopic expression of HES1. *Hes1*-KO MSCs transfected with NFATc2-luciferase reporter showed robust luciferase activity induced by LPS treatment (Fig 7B). Ectopic expression of HES1 significantly suppressed NFATc2-luciferase reporter activity. These results indicate that HES1 is required for repression of NFATc2 promoter transcription.

To provide additional evidence for the ability of HES1 in repressing NFATc2 promoter activity, we performed a chromatin immunoprecipitation (ChIP) and analyzed HES1 occupancy in the 5'-flanking regions of the NFATC2 gene, extending from approximately 2.5 kb to the transcription start site (TSS). We detected strong inflammation-responsive binding of HES1 in the previously characterized B class E box (CANGTG, -2256 & -487) and weaker binding to the N class E box (CACNAG, -1760) in the NFATC2 promoter (Fig 7C), with consensus HES1-binding sites (36, 45, 46). These results provide biochemical evidence that HES1 binds to on the regulatory region of the *Nfatc2* gene (Fig 7D), to suppress NFATc2-mediated inflammation in BM MSCs (Fig 7E).

Discussion

The long-term maintenance of functional hematopoietic stem cells (HSCs) intricately tied to their native tissue microenvironment within the bone marrow (BM; 1, 2). One key player in regulating this environment is HES1, a transcriptional repressor encoded by the *Notch target gene Hairy and Enhancer of Split-1*. While HES1 has long been associated with cellular processes like proliferation and differentiation during embryogenesis (7), its role in the BM microenvironment, particularly regarding mesenchymal stromal cells (MSCs), has remained less understood. In this study, we demonstrate that HES1 regulates BM MSC function through suppressing NFATc2-mediated inflammation in the BM niche. Our study provides several lines of evidence to supporting this conclusion: 1) HES1 is essential for MSC self-renewal *in vitro*; 2) *Hes1* deficiency impairs the hematopoietic supportive function of MSC both *in vitro* and *in vivo*; 3) *Hes1* loss disrupts transcriptional programs, leading to enhanced stromal

inflammation and MSC dysfunction; 4) Inhibition of inflammation rescues *Hes1*-deficient MSC function; and 5) Mechanistically, HES1 binds to E-boxes in NFATc2 promoter, repressing NFATc2-mediated inflammatory cytokine production in the BM microenvironment.

One interesting finding of the present study is that *Hes1* deletion in the BM leads to a reduction in MSC frequency and impairs MSC self-renewal. HES1 has been shown to directly control cell proliferation through the transcriptional repression of $p27^{Kip1}$ (47). Our previous studies also demonstrated that HES1 regulates fetal hematopoiesis through suppressing p27 and PTEN expression (21). While further investigation is needed to explore the underlying mechanisms, the current findings underscore the role of HES1 in MSC homeostasis, particularly in preserving their proliferative capacity and functional integrity through the modulation of gene expression.

We did not observe significant changes in blood parameters in the naïve *Hes1*$^{fl/fl}$*Prx1Cre* mice, indicating that mesenchymal HES1 is not essential for maintaining steady-state hematopoiesis. However, the hypersensitivity of *Hes1*$^{fl/fl}$*Prx1Cre* mice to LPS-induced inflammation aligns with previous studies suggesting that MSCs are essential for supporting hematopoiesis under stress conditions by modulating inflammation (48). MSCs exert immunosuppressive and anti-inflammatory functions through the secretion of cytokines and growth factors that regulate the BM microenvironment and promote HSC survival and differentiation (49). Loss of HES1 disrupts these processes, impairing the capacity of MSCs to support hematopoiesis in inflammatory conditions. Our findings emphasize the critical role of HES1 in modulating MSC responses to inflammatory stimuli. This study contributes to

the growing body of research highlighting the importance of the BM microenvironment in regulating hematopoiesis, with MSCs as key modulators, especially under stress or inflammation. Previous research has shown that MSCs influence hematopoiesis through direct interactions and cytokine secretion, such as interleukins and TNF-α, vital for maintaining HSC function. Our current findings extend this understanding by identifying HES1 as a crucial regulator of MSC-mediated hematopoietic support, through the regulation of inflammatory pathways.

At the molecular level, our transcriptomic analysis of HES1-deficient MSCs reveals significant alterations in gene expression, particularly in genes associated with cellular metabolism and inflammation (Fig 5). Among them, we identify NFATc2, a transcription factor involved in inflammation and cellular differentiation, as a key target of HES1 regulation (Fig 6). Our data demonstrate that HES1 directly binds to two B-class E boxes and one N class E box within the NFATc2 promoter, thereby suppressing NFATc2-mediated inflammation (Fig 7). This suggests a model in which HES1 acts to repress excessive inflammation within the BM microenvironment, thus preserving MSC homeostasis and their ability to support hematopoiesis. These findings position inflammation as a central factor in MSC dysfunction, offering a potential therapeutic avenue for restoring MSC function in the context of HES1 deficiency. Furthermore, our results align with previous studies implicating NFATc2 in regulating inflammation in the BM microenvironment (50). NFAT signaling has been shown to influence MSC differentiation and function, with dysregulation contributing to pathological conditions such as BM fibrosis and leukemia (50). By identifying HES1 as a negative regulator of

NFATc2, our study unveils a novel mechanism by which MSCs maintain their functional integrity under stress, thereby ensuring the preservation of hematopoiesis.

NFATc2 has increasingly been recognized as a promising therapeutic target across multiple solid tumor types. Our findings connecting NOTCH target, HES1 and NFATc2 contribute critical new evidence that reinforces its functional significance and broadens its potential application in clinical therapy. Furthermore, given the pivotal roles of the Wnt and TGF-β signaling pathways in regulating MSC maintenance and lineage commitment, although further investigation remains to be needed, elucidating the interplay between these pathways within the BM microenvironment may uncover novel mechanisms of tumor-stroma crosstalk and identify additional therapeutic opportunities. In summary, this study highlights an essential role of HES1 in regulating MSC homeostasis and their ability to support hematopoiesis, particularly under inflammatory conditions. By revealing that HES1 modulates the inflammatory response through the suppression of NFATc2, we provide new insights into the molecular mechanisms governing MSC function in the BM niche. These findings suggest potential therapeutic strategies to enhance MSC function in pathological conditions, such as inflammation-induced hematopoietic defects, through modulation of inflammatory pathways. Future studies will be required to explore how other signaling pathways interact with HES1 in MSCs and their broader implications for hematopoiesis and tissue regeneration.

References:

1. Mercier FE, Ragu C, Scadden DT. The bone marrow at the crossroads of blood and immunity. Nat Rev Immunol. 2012;12(1):49-60.
2. Morrison SJ, Scadden DT. The bone marrow niche for haematopoietic stem cells. Nature. 2014;505(7483):327-334.
3. Himburg HA, Termini CM, Schlussel L, et al. Distinct bone marrow sources of pleiotrophin control hematopoietic stem cell maintenance and regeneration. Cell Stem Cell. 2018;23(3):370-381.
4. Zhou BO, Yu H, Yue R, et al. Bone marrow adipocytes promote the regeneration of stem cells and haematopoiesis by secreting SCF. Nat Cell Biol. 2017;19(8):891-903.
5. Artavanis-Tsakonas S, Rand MD, Lake RJ. Notch signaling: cell fate control and signal integration in development. Science. 1999;284(5415):770-776.
6. Zhang H, Sun W, Li X, et al. Use of Hes1-GFP reporter mice to assess activity of the Hes1 promoter in bone cells under chronic inflammation. Bone. 2016;90:80-89.
7. Liu ZH, Dai XM, Du B. Hes1: a key role in stemness, metastasis and multidrug resistance. Cancer Biol Ther. 2015;16(3):353-359.
8. Lei T, Bi Y, Gao MJ, et al. HES1 inhibits adipogenesis of porcine mesenchymal stem cells via transcriptional repression of FAD24. Domest Anim Endocrinol. 2013;45(1):28-32.
9. Kageyama R, Ohtsuka T, Kobayashi T. The Hes gene family: repressors and oscillators that orchestrate embryogenesis. Development. 2007;134(7):1243-1251.
10. Tomita K, Hattori M, Nakamura E, Nakanishi S, Minato N, Kageyama R. The bHLH gene Hes1 is essential for expansion of early T cell precursors. Genes Dev. 1999;13(9):1203-1210.
11. Ma Z, Xu J, Wu L, et al. Hes1 deficiency causes hematopoietic stem cell exhaustion. Stem Cells. 2020;38(6):756-768.
12. Mitchell CA, Verovskaya EV, Calero-Nieto FJ, et al. Stromal niche inflammation mediated by IL-1 signalling is a targetable driver of haematopoietic ageing. Nat Cell Biol. 2023;25(1):30-41.
13. Mitroulis I, Kalafati L, Bornhauser M, Hajishengallis G, Chavakis T. Regulation of the Bone Marrow Niche by Inflammation. Frontier in immunology. Front Immunol. 2020;11:1540.
14. Du W, Adam Z, Rani R, Zhang X, Pang Q. Oxidative stress in Fanconi anemia hematopoiesis and disease progression. Antioxid Redox Signal. 2008;10(11):1909-1921.
15. Pan MG, Xiong Y, Chen F. NFAT Gene Family in Inflammation and Cancer. Curr Mol Med. 2013;13(4):543-554.
16. Weigmann B, Lehr HA, Yancopoulos G, et al. The transcription factor NFATc2 controls IL-6-dependent T cell activation in experimental colitis. J Exp Med. 2008;205(9):2099-2110.

17. Fric J, Zelante T, Wong AYW, Mertes A, Yu HB, Ricciardi-Castagnoli P. NFAT control of innate immunity. Blood. 2012;120(7):1380-1389.
18. Urso K, Alfranca A, Martinez-Martinez S, et al. NFATc3 regulates the transcription of genes involved in T-cell activation and angiogenesis. Blood. 2011;118(3):795-803.
19. Williamson M, Damm E, Clements W. NFAT transcription factors are required for definitive hematopoiesis. Exp Hematol. 2023;124:S160.
20. Arabanian LS, Haase M, Habermann I, et al. Lack of the Transcription Factor NFAT (Nuclear Factor of Activated T cells) c2 in Hematopoietic Progenitor Cells Results in Profound Hematological Abnormalities in Mice. Blood. 2011;18(21):1296.
21. Zhu AZ, MA Z, Wolff EV, Lin Z, Gao ZJ, Du W. HES1 is required for mouse fetal hematopoiesis. Stem Cell Res Ther. 2024;15(1):235.
22. Kfoury Y, Scadden DT. Mesenchymal cell contributions to the stem cell niche. Cell Stem Cell. 2015;16(3):239-253.
23. Ding L, Morrison SJ. Haematopoietic stem cells and early lymphoid progenitors occupy distinct bone marrow niches. Nature. 2013;495(7440):231-235.
24. Xu J, Li X, Cole A, Sherman Z, Du W. Reduced Cell Division Control Protein 42 Activity Compromises Hematopoiesis-Supportive Function of Fanconi Anemia Mesenchymal Stromal Cells. Stem Cells. 2018;36(5):785-795.
25. Lin Q, Wu L, Ma Z, Chowdhury FA, Mazumder HH, Du W. Persistent DNA damage-induced NLRP12 improves hematopoietic stem cell function. JCI insight. 2020;5(10);e133365.
26. Uddin M, Betts C, Robinson I, Malmgren A, Humfrey C. The chemokine CXCR2 antogonist (AZD5069) preserves neutrophil-mediated host immunity in no-human primates. Haematologica. 2017;102(2):e65-e68.
27. Li S, Kang P, Zhang W, et al. Activated NLR family pyrin domain containing 3 (NLRP3) inflammasome in keratinocytes promotes cutaneous T-cell response in patients with vitiligo. J Allergy Clin Immunol. 2020;145(2):632-645.
28. Neighbour H, Boulet LP, Lemiere C, et al. Safety and efficacy of an oral CCR3 antagonist in patients with asthma and eosinophilic bronchitis: a randomized, placebo-controlled clinical trial. Clin Exp Allergy. 2014;44(4):508-516.
29. Rathod S, Ramsey M, Finkelman FD, Fernandez CA. Genetic inhibition of NFATC2 attenuates asparaginase hypersensitivity in mice. Blood Adv. 2020;4(18):4406-4416.
30. Kobayashi M, Srour EF. Regulation of murine hematopoietic stem cell quiescence by Dmtf1. Blood. 2011;118(25):6562-6571.
31. Sejas DP, Rani R, Qiu Y, et al. Inflammatory reactive oxygen species-mediated hemopoietic suppression in Fancc-deficient mice. J Immunol. 2007;178(8):5277-5287.
32. Barry F, Murphy M. Mesenchymal stem cells in joint disease and repair. Nat Rev Rheumatol. 2013;9(10):584-594.
33. Zhang P, Chen Z, Li R, et al. Loss of ASXL1 in the bone marrow niche dysregulates hematopoietic stem and progenitor cell fates. Cell Discov. 2018;4:4.

34. Pittenger MF, Mackay AM, Beck SC, et al. Multilineage potential of adult human mesenchymal stem cells. Science. 1999;284(5411):143-147.
35. Mendez-Ferrer S, Michurina TV, Ferraro F, et al. Mesenchymal and haematopoietic stem cells form a unique bone marrow niche. Nature. 2010;466:829-834.
36. Wu L, Li X, Lin Q, Chowdhury F, Mazumder MH, Du W. FANCD2 and HES1 suppress inflammation-induced PPAR to prevent haematopoietic stem cell exhaustion. Br J Haematol. 2021;192(3):652-663.
37. Mercatelli D, Lopez-Garcia G, Giorgi FM. *corto*: a lightweight R package for gene network inference and master regulator analysis. Bioinformatics. 2020;36(12):3916-3917.
38. Subramanian A, Tamayo P, Mootha VK, et al. Gene set enrichment analysis: a knowledge-based approach for interpreting genome-wide expression profiles. Proc Nat Acad Sci. 2005;102(43):15545-15550.
39. Yamashita M, Passegue E. TNFα coordinates hematopoietic stem cell survival and myeloid regeneration. Cell Stem Cell. 2019;25(3):357-372.
40. Sinclair A, Park L, Shah M, et al. CXCR2 and CXCL4 regulate survival and self-renewal of hematopoietic stem/progenitor cells. Blood. 2016;128(3):371-383.
41. Eash KJ, Greenbaum AM, Gopalan PK, Link DC. CXCR2 and CXCR4 antagonistically regulate neutrophil trafficking from murine bone marrow. J Clin Invest. 2010;120(7):2423-2431.
42. Villatoro A, Cuminetti V, Bernak A, et al. Endogenous IL-1 receptor antagonist restricts healthy and malignant myeloproliferation. Nat Commu. 2023;14(1):12.
43. Miyaki T, Sugaya M, Murakami T, et al. CCL11-CCR3 Interactions Promote Survival of Anaplastic Large Cell Lymphoma Cells via ERK1/2 Activation. Cancer Res. 2011;71(6):2056-2065.
44. Ichida M, Finkel T. Ras regulates NFAT3 activity in cardiac myocytes. J Biol Chem. 2001;276(5):3524-3530.
45. Herzig S, Hedrick S, Morantte I, Koo SH, Galimi F, Montminy M. CREB controls hepatic lipid metabolism through nuclear hormone receptor PPAR-gamma. Nature. 2003;426(6963):190-193.
46. Iso T, Kedes L, Hamamori Y. HES and HERP families: multiple effectors of the Notch signaling pathway. J Cell Physiol. 2003;194(3):237-255.
47. Murata K, Hattori M, Hirai N, et al. Hes1 directly controls cell proliferation through the transcriptional repression of p27Kip1. Mol Cell Biol. 2005;25(10):4262-4271.
48. Dabrowska S, Andrzejewska A, Jonawski M, Lukomska B. Immunomodulatory and Regenerative Effects of Mesenchymal Stem Cells and Extracellular Vesicles: Therapeutic Outlook for Inflammatory and Degenerative Diseases. Front Immunol. 2021;11:591065.
49. Najar M, Melki R, Khalife E, et al. Therapeutic Mesenchymal Stem/Stromal Cells: Value, Challenges and Optimization. Frontiers Cell Dev Biol. 2022;9:716853.
50. Pimenta DB, Varela VA, Datoguia TS, et al. The Bone Marrow Microenvironment Mechanisms in Acute Myeloid Leukemia. Frontiers Cell Dev Biol. 2021;9:764698.

Figure legend

Fig 1. *Hes1* deletion in bone marrow mesenchymal stromal cells does not alter steady state hematopoiesis. A. Bone marrow (BM) cellularity of *Hes1*$^{fl/fl}$*Prx1Cre* and *Hes1*$^{fl/fl}$ mice. Left: representative microscopic H&E images (20X) of bone section of *Hes1*$^{fl/fl}$*Prx1Cre* and *Hes1*$^{fl/fl}$ mice (Left), and mean BM cell counts per femur for each group (right) are shown. B. Comparable hematopoietic stem progenitor cell (HSPC) frequencies in *Hes1*$^{fl/fl}$*Prx1Cre* mice. Whole bone marrow cells (WBMCs) isolated from *Hes1*$^{fl/fl}$*Prx1Cre* and *Hes1*$^{fl/fl}$ mice were subjected to flow cytometry analysis for LSK ($Lin^-Sca1^+c\text{-}kit^+$) and SLAM ($Lin^-Sca1^+c\text{-}kit^+CD48^-CD150^+$) staining. Representative plots (Left) and quantification (Right) are shown. C. *Hes1* deletion slightly alters HSC quiescence. WBMCs from *Hes1*$^{fl/fl}$*Prx1Cre* and *Hes1*$^{fl/fl}$ mice were subjected to flow cytometry analysis for Ki67 and DAPI. SLAM cells were gated for analysis. Representative plots (left) and quantification (right) are shown. D. *Hes1* deficiency does not affect cell viability. Cells described in (A) were gated for SLAM population and analyzed for apoptosis by Annexin V and 7AAD. Representative plots (left) and quantification (right) are shown. Results are mean ± Standard Error of Mean (SEM) of three independent experiments (n = 6/group).

Fig 2. *Hes1*$^{fl/fl}$*Prx1Cre* mice are hypersensitivity to LPS challenge. A. *Hes1*$^{fl/fl}$*Prx1Cre* mice are hypersensitive to LPS-induced septic shock. Kaplan-Meier survival curves are shown for a single dose (25 mg/kg) of intraperitoneally (i.p.) injected LPS. Experiments were repeated three times, each with 6 animals (total 18 mice) for *Hes1*$^{fl/fl}$*Prx1Cre* or *Hes1*$^{fl/fl}$ mice (10~14 weeks old). The log rank test indicated a statistically significant difference ($p = 0.0019$) in survival between the two genotype

groups. B. LPS reduces blood counts in *Hes1*$^{fl/fl}$*Prx1Cre* mice. *Hes1*$^{fl/fl}$*Prx1Cre* and *Hes1*$^{fl/fl}$ mice were injected intraperitoneally (i.p.) with LPS in PBS at a single dose of 1 mg/kg. Numbers of red blood cells and concentrations of hemoglobin and hematocrit in peripheral blood (PB) were determined on day 3 after the last dose of LPS. C. BM cellularity of *Hes1*$^{fl/fl}$*Prx1Cre* and *Hes1*$^{fl/fl}$ mice 2 days after LPS injection. D. *Hes1*-deficiency compromises hematopoietic recovery *in vivo* following LPS treatment. *Hes1*$^{fl/fl}$*Prx1Cre* and *Hes1*$^{fl/fl}$ mice were injected i.p. with LPS (1 mg/kg). Red blood cell counts were conducted for 10 days after injection. E. Mouse PB parameters after LPS injection. Complete blood count (CBC) was performed using PB from mice administered with LPS. Data are expressed as mean ± SD of two independent experiments, each with 6 animals (total 12 mice).

Fig 3. HES1 is required for BM MSC self-renewal. A. Loss of *Hes1* reduces MSC frequency in the BM. Phenotypic MSC ($CD45^-CD44^+CD105^+CD73^+CD146^+CD90^+$) frequency in *Hes1*$^{fl/fl}$*Prx1Cre* and *Hes1*$^{fl/fl}$ mice were measured by flow cytometry. Representative flow plots (Left) and quantification (Right) are shown. B. MSCs from *Hes1*$^{fl/fl}$*Prx1Cre* mice exhibit defective proliferation *in vitro*. MSCs isolated from *Hes1*$^{fl/fl}$*Prx1Cre* and *Hes1*$^{fl/fl}$ littermates were cultured in MSC medium followed by MSC colony forming efficiency (CFU-F) assay. Numbers of colonies were enumerated on day 12 in triplicate from five individual *Hes1*$^{fl/fl}$*Prx1Cre* and WT mice. Representative images (Left) and quantifications (Right) of CFU-F produced by Passage 0 MSCs are shown. C. Osteoblast differentiation of MSCs from *Hes1*$^{fl/fl}$*Prx1Cre* mice. MSCs isolated from *Hes1*$^{fl/fl}$*Prx1Cre* and *Hes1*$^{fl/fl}$ mice were cultured in osteogenic differentiation medium (MesenCult medium supplemented with 10^{-7} M dexamethasone, 50 μg/ml ascorbic acid

and 10 μM β-glycerophosphate) for 1 week followed by ALP activity staining using a Leukocyte Alkaline Phosphatase Kit. Representative images (Upper) and quantification (Lower) are shown. D. MSCs from *Hes1*$^{fl/fl}$*Prx1Cre* mice display comparable biosynthesis of total lipids. MSCs isolated from the BM of *Hes1*$^{fl/fl}$*Prx1Cre* and *Hes1*$^{fl/fl}$ mice were culture in audiogenic differentiation medium for 2 weeks. Adipocytes were determined by Oil Red O staining. Representative images (Left, 100X magnification) and quantifications (Right) are shown. Absorbance of Oil Red O stain collected from the stained cells by dissolving in 100% isopropanol was measured at 500 nm and blanked to 100% isopropanol.

Fig 4. Loss of *Hes1* compromises hematopoiesis supportive function of MSCs. A. Schematic presentation of *in vitro* experimental design. B. *Hes1*-KO MSCs exhibit reduced Cobblestone area-forming capacity (CAFC). Sorted LSK (Lin$^-$Sca1$^+$c-kit$^+$) cells from WT mice were added onto confluent *Hes1*$^{fl/fl}$*Prx1Cre* and *Hes1*$^{fl/fl}$ mice BM-derived MSCs and incubated at 37ºC. Phase contrast micrographs of differentiating clones after two-week coculture. Maturing hematopoietic cells appear as small refractive (phase bright) cells on the interface of stromal cells and the supernatant. The phase dull cells are cobblestone cells, which are covered by the adherent stromal layer. Representative images (Left) and quantification (Right) are shown. The area was measured in pixels using ImageJ, and plotted as arbitrary units (AU). C. WT cells co-cultured with *Hes1*-KO MSCs are defective in CFU assay. Progenies from B were subjected to CFU assay. Colonies were enumerated on day 7. D. *Hes1*-KO MSC co-cultured WT progenies are less functional in reconstituting recipient mice. Progenies from B were subjected to BMT, along with 2X10^5 competitor cells from BoyJ mice. Donor-derived chimera was

measured by flow cytometry 16 weeks post BMT. Representative flow plots (Left) and quantifications (Right) are shown. E, F. *Hes1*$^{fl/fl}$*Prx1Cre* MSCs fail to support long-term hematopoiesis. WBMCs isolated from primary recipients described in (D) at 16 weeks post-transplant was transplanted into sublethally irradiated BoyJ recipients. Donor-derived chimera (Total CD45.2^{+}; E) and percentages of LSK, SLAM cells in the donor-derived (Total CD45.2^{+}) cell compartment (F) were determined at 16-weeks post-transplant. Representative flow plots and quantifications are shown. G. Schematic presentation of reverse BMT design. H. MSCs deficient for *Hes1* are defective in supporting hematopoiesis *in vivo*. WBMCs from BoyJ mice (CD45.1^{+}) were transplanted into lethally irradiated *Hes1*$^{fl/fl}$*Prx1Cre* and *Hes1*$^{fl/fl}$ mice. Donor-derived chimera was measured by flow cytometry at different time points. Results are means ± standard deviation (SD) of three independent experiments (n= 6~9 per group).

Fig 5. *Hes1* deletion alters the expression of gene critical for inflammation. (A) *Hes1*-KO altered a gene expression profile in mouse MSC. Hierarchical clustering illustrates large-scale differences in genes between *Hes1*-KO vs control MSCs. (B) Enrichment plots of Hallmark pathways up-regulated in *Hes1*-KO MSCs. (C) Network visualization of GSEA in Hallmark. Blue nodes represent down-regulated and red nodes represent up-regulated Hallmark pathways in *Hes1*-KO group. Node color intensity, node size, and edge thickness are proportional to value of normalized enrichment score (NES), the number of genes in gene signature, and the number of overlapping genes between two connected nodes. (D) MRA result summary; the heatmap shows the differences in gene expression levels of the 7 MRs in *Hes1*-KO vs control groups. Bar graph shows the distribution of positively (red) or negatively (blue) correlated target

genes of the MRs (Spearman's correlation between the expression levels of the MR and its targets). The mode on the right explains whether *Hes1*-KO positively (+) or negatively (−) affects the expression of MRs.

Fig 6. Blocking inflammation restores *Hes1*$^{fl/lf}$*Prx1Cre* MSC function. A. Inhibition of TNF-α, CXCR2, IL-1β or CCR3 improves CFU-F activity of *Hes1*$^{fl/fl}$*Prx1Cre* MSCs. MSCs from *Hes1*$^{fl/fl}$*Prx1Cre* or *Hes1*$^{fl/fl}$ mice were cultured *ex vivo* in the presence or absence of the indicated inhibitors followed by CFU-F assays. Qualifications are shown. B-D. Blocking inflammation improves hematopoiesis supportive function *Hes1*-KO MSCs *in vitro*. MSCs described in (A) were subjected to CAFC assay (B), CFU (C) and BMT (D). E. TNF-α, CXCR2, IL-1β or CCR3 blockade improves hematopoiesis supportive function of *Hes1*-KO MSCs *in vivo*. WBMCs from BoyJ mice (CD45.1^{+}) were transplanted into lethally irradiated *Hes1*$^{fl/fl}$*Prx1Cre* and *Hes1*$^{fl/fl}$ mice, followed by i.p. injection of TNF-α, CXCR4, IL-1β or CCR3. Results are means ± SD of 3 independent experiments (n=9 per group). *, $p<0.05$, **, $p<0.01$.

Fig 7. HES1 binds to NFATc2 promoter to suppress its activity. A. Inhibition of NFATc2 reduces stomal inflammation in *Hes1*-KO MSCs. MSCs from *Hes1*$^{fl/fl}$*Prx1Cre* mice or their *Hes1*$^{fl/fl}$ littermates were cultured in the presence or absence of NFATc2 inhibitor, 11-VIVIT, followed by ELISA for the indicated cytokines. Quantifications are shown. B. HES1 represses NFATc2 expression. MSCs from *Hes1*$^{fl/fl}$*Prx1Cre* mice expressing a NFATc2 reporter construct containing 1.5 kB of the proximal NFATc2 promoter were co-transfected with HES1 expressing vectors. Subsequently, cells were treated with LPS (50 ng/ml) or vehicle followed by luciferase activity analysis. C. HES1 binds to NFATc2 promoter. ChIP assays were carried out using anti-HES1 antibody or

IgG. The regions encompassing the HES1-binding sites in the previously characterized B Class E box (CANGTG) and N Class E box (CANGTG) in the NFATc2 promoter were amplified by real-time PCR. Results were means ±SD of three independent experiments. D. Sequences of the consensus HES1-binding sites in the NFATc2 promoter. +1 indicates transcription start site, TSS, E-Boxes, and a HES1-binding site were indicated. E. Working model. HES1 regulates MSC function through suppressing NFATc2-mediated inflammation.

Fig 1

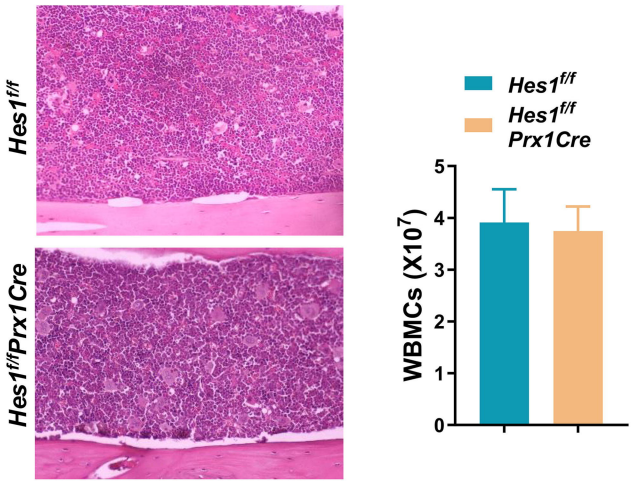
A
Hes1f/f
Hes1f/fPrx1Cre
Hes1f/f
Hes1f/f Prx1Cre
WBMCs (X10^7)
0
1
2
3
4
5

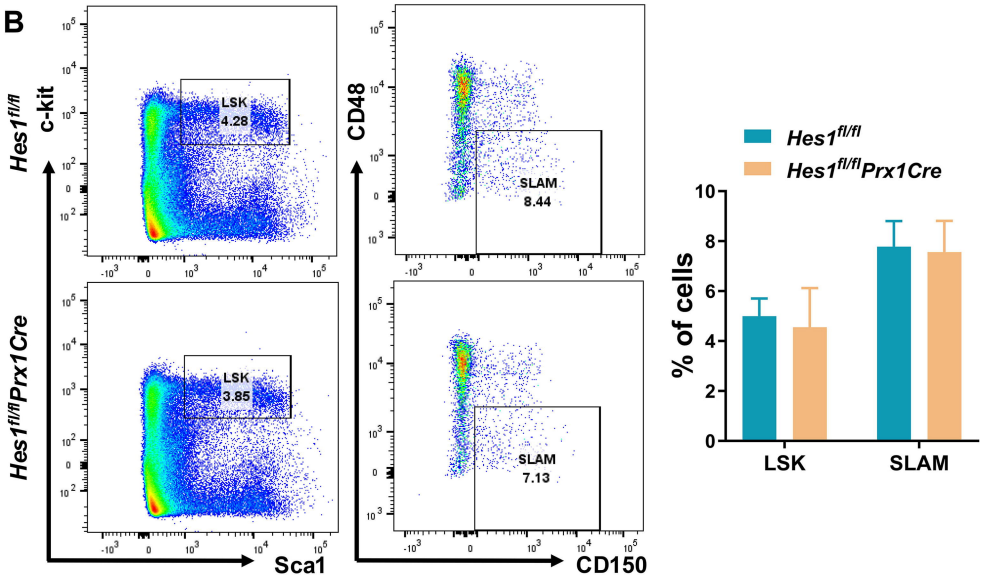
B
Hes1fl/fl
Hes1fl/flPrx1Cre
c-kit
Sca1
LSK
4.28
LSK
3.85
CD48
CD150
SLAM
8.44
SLAM
7.13
Hes1fl/fl
Hes1fl/flPrx1Cre
% of cells
0
2
4
6
8
10
LSK
SLAM

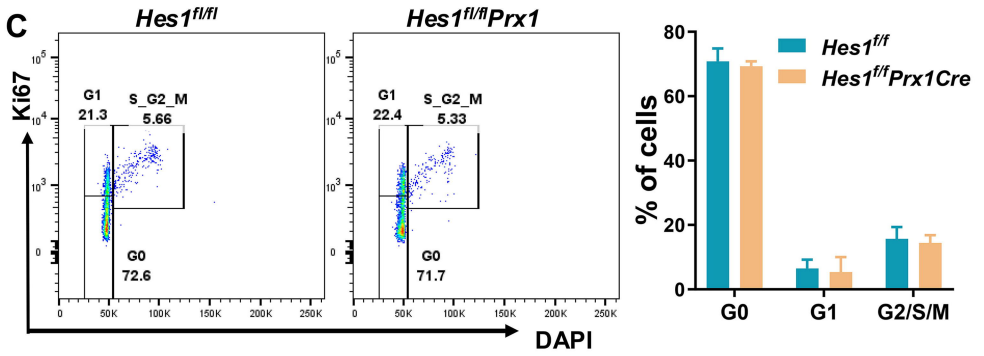
C
Hes1fl/fl
Hes1fl/flPrx1
Ki67
DAPI
G1
21.3
S_G2_M
5.66
G0
72.6
G1
22.4
S_G2_M
5.33
G0
71.7
Hes1f/f
Hes1f/fPrx1Cre
% of cells
0
20
40
60
80
G0
G1
G2/S/M

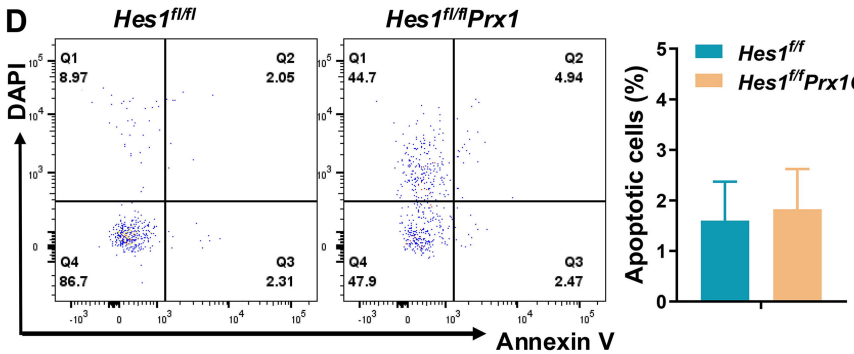
D
Hes1fl/fl
Hes1fl/flPrx1
DAPI
Annexin V
Q1
8.97
Q2
2.05
Q4
86.7
Q3
2.31
Q1
44.7
Q2
4.94
Q4
47.9
Q3
2.47
Hes1f/f
Hes1f/fPrx1Cre
Apoptotic cells (%)
0
1
2
3
4
5

Fig 2

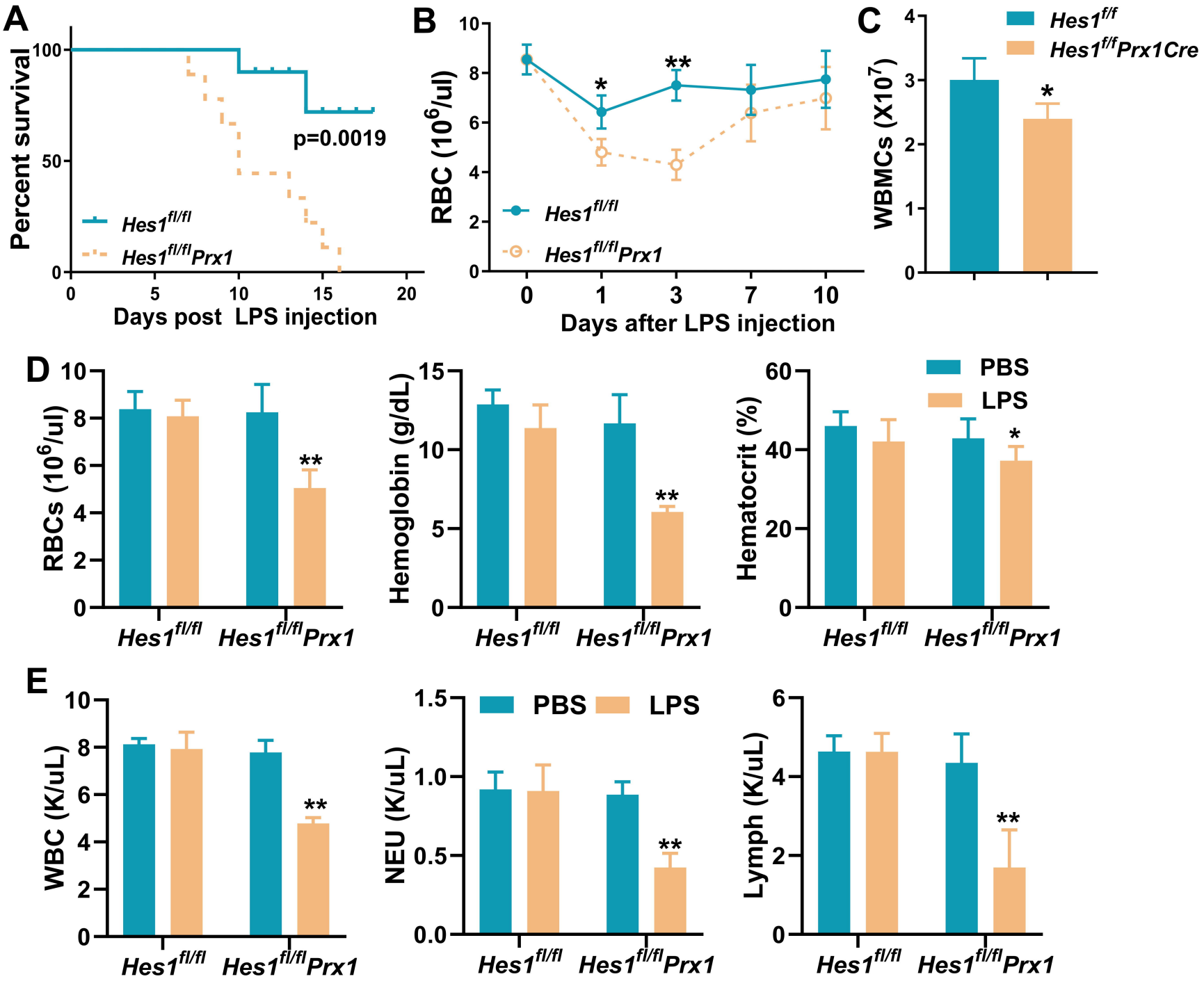
A
Percent survival
100
50
0
p=0.0019
Hes1fl/fl
Hes1fl/flPrx1
0
5
10
15
20
Days post LPS injection
B
RBC (10^6/ul)
10
8
6
4
2
0
*
**
Hes1fl/fl
Hes1fl/flPrx1
0
1
3
7
10
Days after LPS injection
C
WBMCs (X10^7)
4
3
2
1
0
Hes1f/f
Hes1f/fPrx1Cre
*
D
RBCs (10^6/ul)
10
8
6
4
2
0
**
Hes1fl/fl
Hes1fl/flPrx1
Hemoglobin (g/dL)
15
10
5
0
**
Hes1fl/fl
Hes1fl/flPrx1
Hematocrit (%)
60
40
20
0
PBS
LPS
*
Hes1fl/fl
Hes1fl/flPrx1
E
WBC (K/uL)
10
8
6
4
2
0
**
Hes1fl/fl
Hes1fl/flPrx1
NEU (K/uL)
1.5
1.0
0.5
0.0
PBS
LPS
**
Hes1fl/fl
Hes1fl/flPrx1
Lymph (K/uL)
6
4
2
0
**
Hes1fl/fl
Hes1fl/flPrx1

Fig 3. Loss of Hes1 in BM niche affect MSC self-renewal

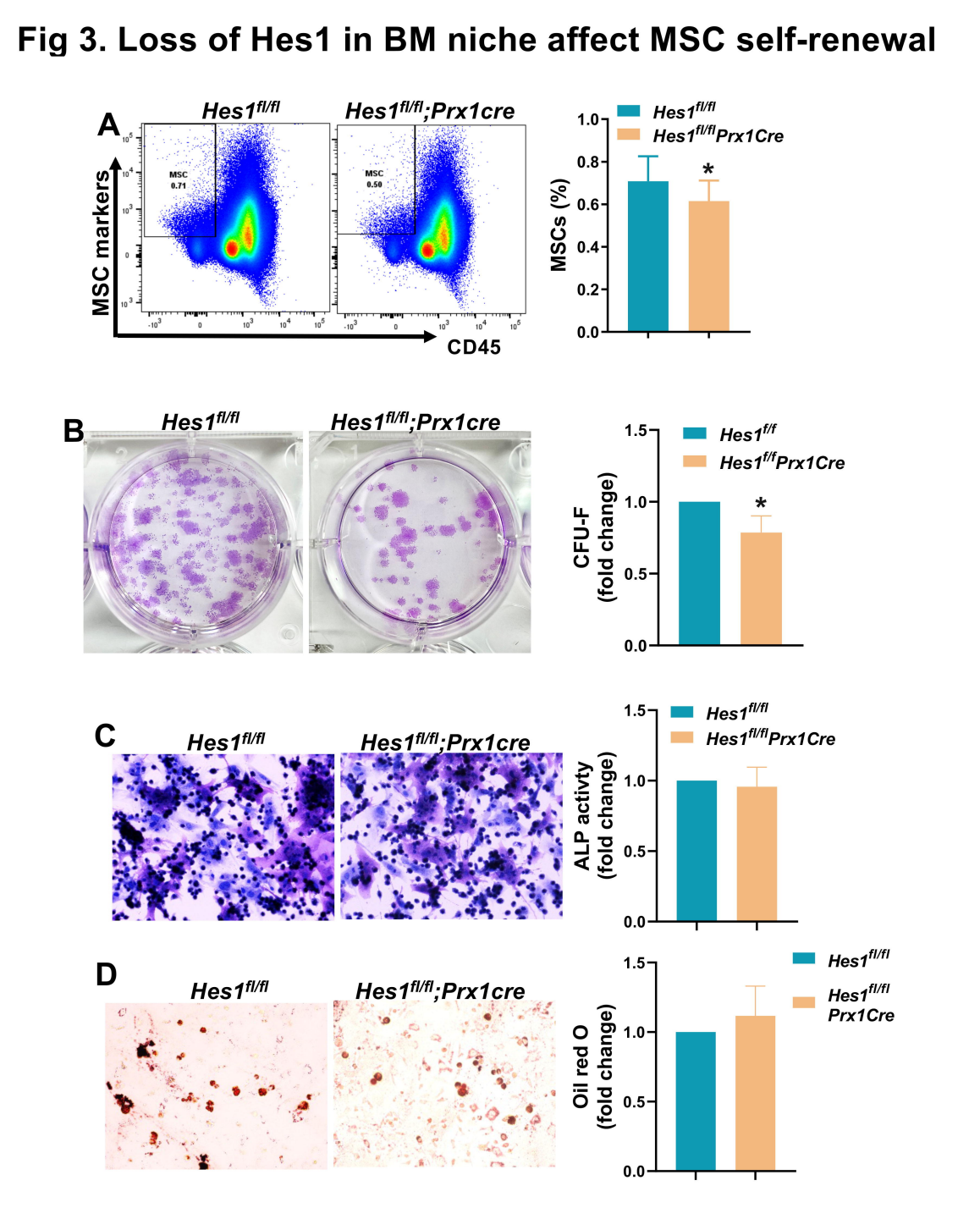

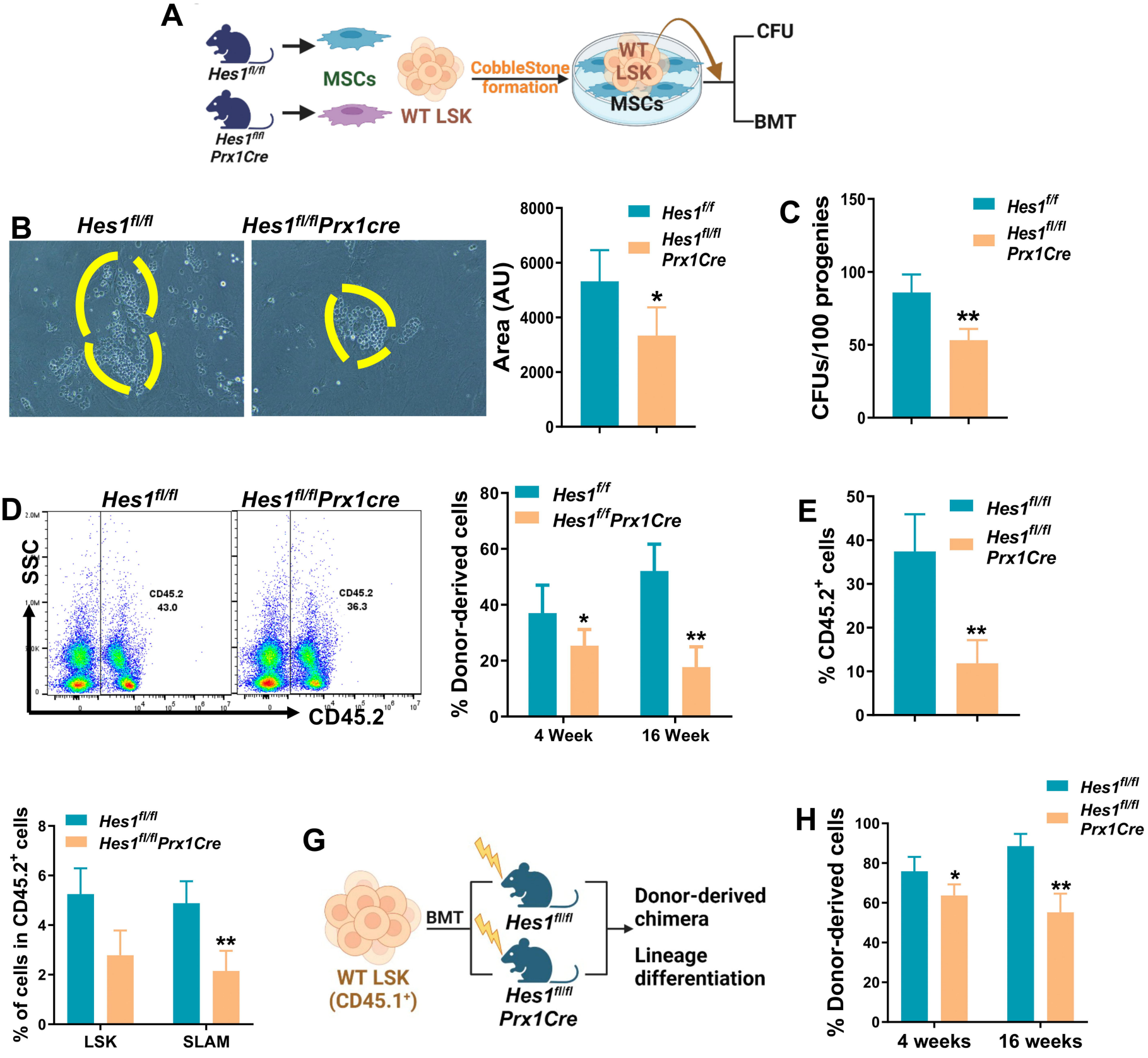
A
Hes1fl/fl
MSCs
Hes1fl/fl Prx1Cre
WT LSK
CobbleStone formation
WT LSK
MSCs
CFU
BMT
B
Hes1fl/fl
Hes1fl/flPrx1cre
Area (AU)
Hes1f/f
Hes1fl/fl Prx1Cre
C
CFUs/100 progenies
D
Hes1fl/fl
Hes1fl/flPrx1cre
SSC
CD45.2
43.0
CD45.2
36.3
CD45.2
% Donor-derived cells
Hes1f/f
Hes1f/fPrx1Cre
4 Week
16 Week
E
% CD45.2+ cells
F
% of cells in CD45.2+ cells
Hes1fl/fl
Hes1fl/flPrx1Cre
LSK
SLAM
G
WT LSK
(CD45.1+)
BMT
Hes1fl/fl
Hes1fl/fl Prx1Cre
Donor-derived chimera
Lineage differentiation
H
% Donor-derived cells
4 weeks
16 weeks

Figure 5

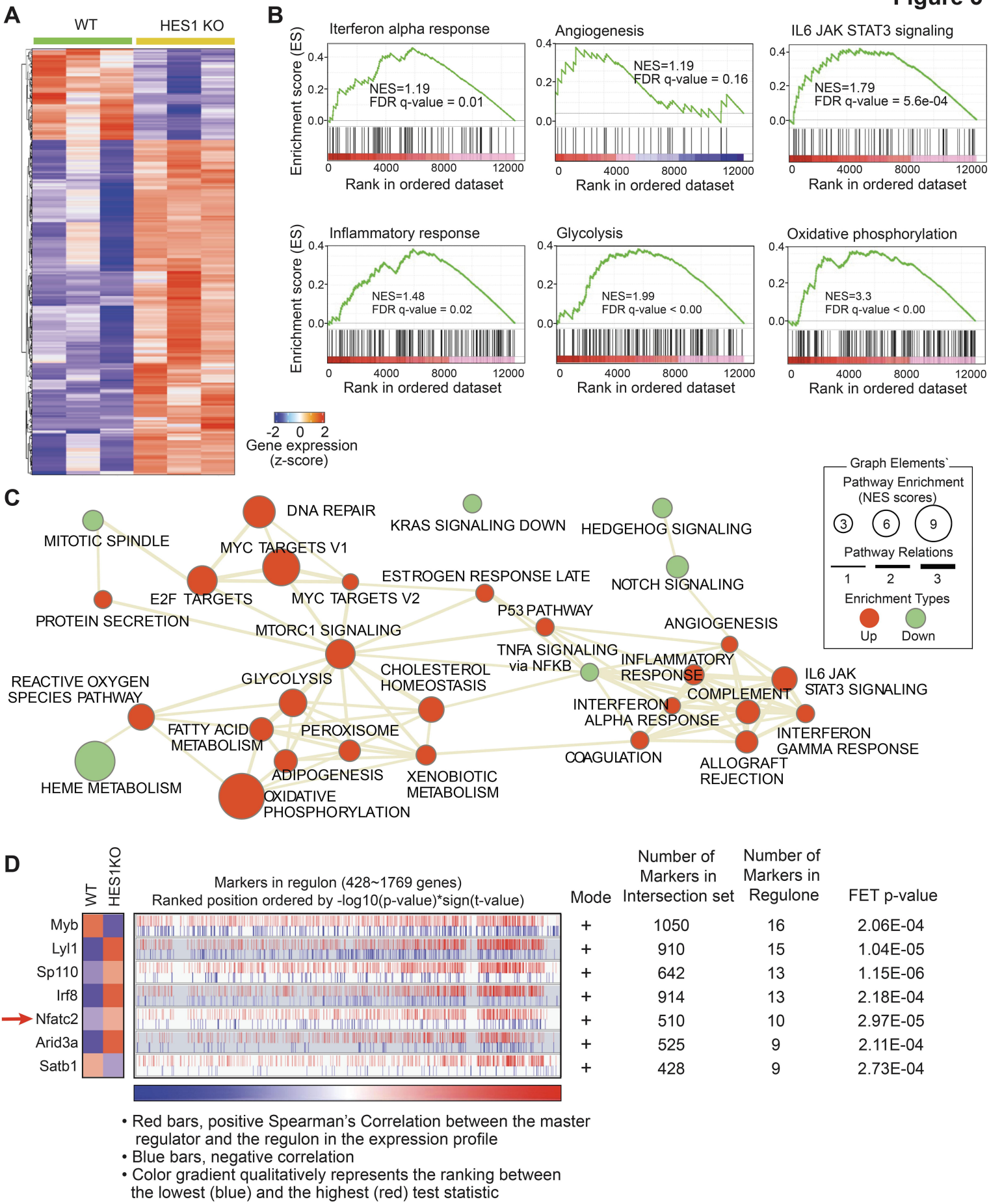

	Mode	Number of Markers in Intersection set	Number of Markers in Regulone	FET p-value
Myb	+	1050	16	2.06E-04
Lyl1	+	910	15	1.04E-05
Sp110	+	642	13	1.15E-06
Irf8	+	914	13	2.18E-04
Nfatc2	+	510	10	2.97E-05
Arid3a	+	525	9	2.11E-04
Satb1	+	428	9	2.73E-04

Figure 6

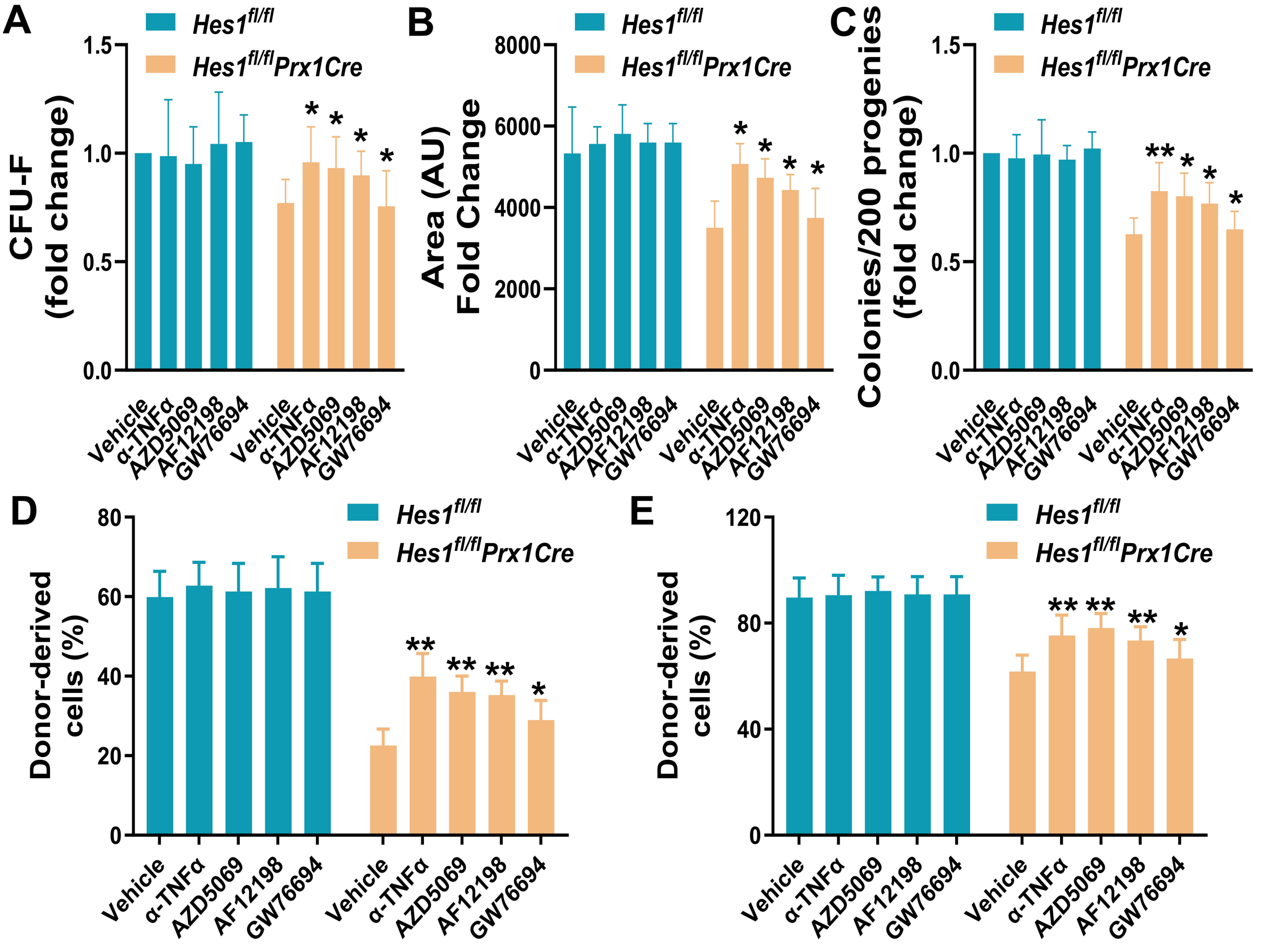
A
B
C
D
E
Hes1fl/fl
Hes1fl/flPrx1Cre
CFU-F (fold change)
Area (AU) Fold Change
Colonies/200 progenies (fold change)
Donor-derived cells (%)
Donor-derived cells (%)
Vehicle
α-TNFα
AZD5069
AF12198
GW76694

Fig 7

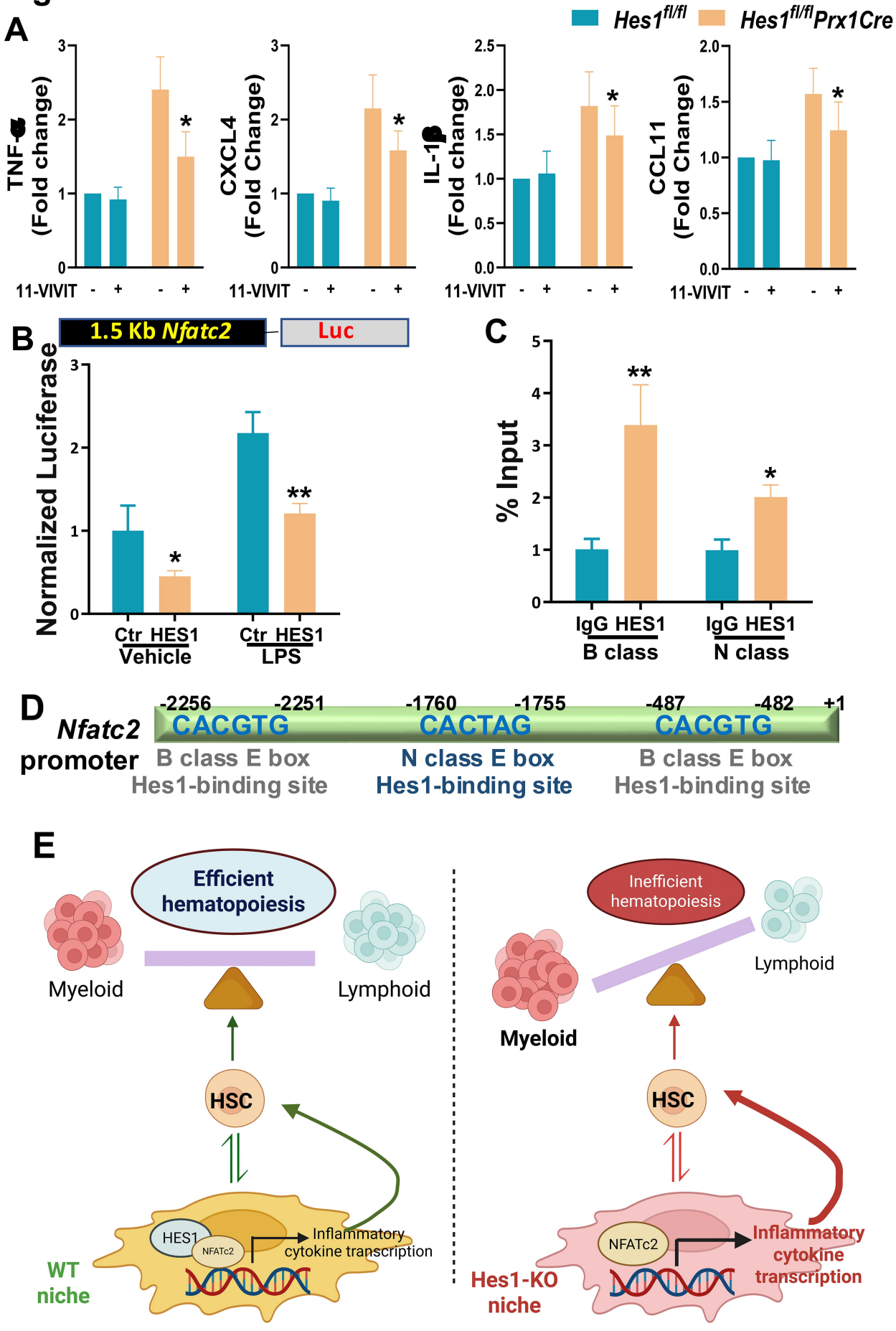
A
Hes1fl/fl
Hes1fl/flPrx1Cre
TNF-α (Fold change)
CXCL4 (Fold Change)
IL-1β (Fold change)
CCL11 (Fold Change)
11-VIVIT - + - +
B
1.5 Kb Nfatc2
Luc
Normalized Luciferase
Ctr HES1
Vehicle
Ctr HES1
LPS
C
% Input
IgG HES1
B class
IgG HES1
N class
D
Nfatc2 promoter
-2256
-2251
-1760
-1755
-487
-482
+1
CACGTG
CACTAG
CACGTG
B class E box Hes1-binding site
N class E box Hes1-binding site
B class E box Hes1-binding site
E
Efficient hematopoiesis
Myeloid
Lymphoid
HSC
HES1
NFATc2
Inflammatory cytokine transcription
WT niche
Inefficient hematopoiesis
Myeloid
Lymphoid
HSC
NFATc2
Inflammatory cytokine transcription
Hes1-KO niche

Supplementary material

Flow cytometry

Bone marrow (BM) mesenchymal stroma cell (MSC) populations were stained with fluorescently labelled antibodies for mesenchymal (CD29, CD44, CD73, SCA-1, CD106) and hematopoietic markers (CD45, CD11b) using the mouse multipotent mesenchymal stromal cell marker antibody panel (Cat # SC018; R&D systems; Minneapolis, MN; 1-3). We confirmed that at least 98% MSC purity was obtained with this culture method.

For donor derived chimera analysis, peripheral blood (PB) from the recipient mice were subjected to staining using PE-anti-CD45.1, APC-anti-CD45.2 (Both from BD Biosciences, Cat #: 553776 and 558702, San Jose, CA) antibodies followed by Flow cytometry analysis.

For apoptosis staining, surface marker-stained cells were incubated with Annexin V and 7AAD using the BD ApoAlert Annexin V Kit (BD Pharmingen, San Jose, CA) in accordance with the manufacturer's instruction. Flow cytometry analysis was then performed to determine the proportion of Annexin V-positive cells.

For cell cycle analysis, cells stained for surface markers were fixed and permeabilized with Cytofix/Cytoperm buffer (BD Pharmingen) followed by intensive wash using Perm/Wash Buffer (BD Pharmingen). Anti-mouse Ki67 antibody (BD Pharmingen) and DAPI (Sigma-Aldrich) were then used to incubate the cells followed by flow cytometry analysis.

MSC Culture and Lineage Differentiation Assays

To measure the frequency of MSCs in the BM, colony forming unit fibroblast (CFU-F) assay was performed as previously described (4). Briefly, $4x10^6$ bone marrow

mononuclear cells (BMMNCs) were plated into 6-well tissue culture plates in triplicate for each condition in mouse MesenCult medium (MesenCult basal media plus 20% of MesenCult Supplemental, Stem Cell Technologies Inc,) and incubated at 37°C and 5% CO_2. After 10 days of culture, medium was removed and each well was washed with phosphate-buffered saline (PBS), stained with 0.5% crystal violet solution (Fisher Scientific Company, VA, USA) according to the manufacturer's instructions and photographed.

For CFU-osteoblast assays, after 7 days of culture, medium was removed and switched to osteogenic differentiation medium (MesenCult medium supplemented with 10^{-7} M dexamethasone, 50 μg/mL ascorbic acid and 10 mM β-glycerophosphate). Medium was changed every other day for one week of continuous culture. Staining for ALP activity was subsequently performed using a Leukocyte Alkaline Phosphatase (ALP) kit according to the manufacturer's instructions (2, 3). Photomicrographs of the stained cells were acquired with a Nikon TE2000-S microscope. The area and intensity of ALP^+ cells were quantified using Image J software.

For CFU-adipocyte assays, after 5 days of culture, medium was changed to adipogenic differentiation medium (MesenCult medium supplemented with 10^{-7} M dexamethasone, 450 μM isobutylmethylxanthine, 1 μg/mL insulin and 200 μM indomethacin). Culture medium changes every 5 days for 4 weeks. Adipocytes were determined by Oil Red O staining (5, 6).

RNA-seq data generation and pre-process

Qiagen RNeasy kit was used to extract total RNA from mouse MSCs. We calculated total RNA concentration and assessed the integrity. A library was independently prepared with

1μg of total RNA for each sample by Illumina TruSeq Stranded mRNA Sample Prep Kit (Illumina, Inc., San Diego, CA, USA, #RS-122-2101). The libraries were quantified using KAPA Library Quantification kits for Illumina Sequencing platforms according to the qPCR Quantification Protocol Guide (KAPA BIOSYSTEMS, KK4854) and qualified using the TapeStation D1000 ScreenTape (Agilent Technologies, 5067-5582). Indexed libraries were then submitted to an Illumina NextSeq Mid-Output sequencing kit (Illumina, Inc., San Diego, CA, USA), and the paired-end (2×50 bp) sequencing was performed by the University of Pittsburgh sequencing core.

The raw RNA-seq data are available through the Gene Expression Omnibus (GEO) database under the accession number GSE296738. For analysis we used Rsubread (Bioconductor release 3.8; 7) to align sequence reads to reference genome and used edgeR (8) and limma (9) R packages (Bioconductor release 3.8) to normalize gene expression level to log2 transcripts per million (TPM) (10). We aligned sequence reads to Mus Musculus genome reference sequence (GCF_000001635.27_GRCm39) downloaded from NCBI assembly database and mapped the aligned sequences to gene symbols. After normalization, we contained only protein-coding genes and removed genes of which expression level is zero across all samples to get 26,938 genes for further pathway analysis.

Functional assessment for DEGs and gene set enrichment analysis

To explore the gene expression profile of the effect of *Hes1* KO in the BM MSC, statistical significance of the differential expression data was determined using DESeq2 and fold change. False discovery rate (FDR) was controlled by adjusting *p* value using Benjamini-Hochberg algorithm. The $\log^2$ fold change and p-value obtained from the comparison of

each group plotted as the volcano plot. Hierarchical clustering analysis was performed using complete linkage and Euclidean distance as a measure of similarity. The significant different expression genes (DEGs) were aggregated using the DESeq2 on read counts and the genes were represented in the hierarchical clustering heatmap using the "complete" distance metric for the clustering algorithm. We used ComplexHeatmap R package for the visualization (11). All data analysis and visualization of differentially expressed genes was conducted using R version 4.3.3 (12).

For deep functional assessment of the enriched gene signatures, the DEGs identified between wild type and *Hes1* KO were applied to Gene Signature Enrichment Analysis (GSEA) with Hallmark gene signatures (version 6.2 at MSigDB, http://software.broadinstitute.org/gsea) (13). The pathway network was visualized using the igraph (ver. 2.0.3; 14) and IndepthPathway (ver. 1.0; 15).

Master regulator analysis (MRA) using mouse bone marrow mesenchymal stem cell (MSC)-specific transcriptional interactome

Algorithm for the Reconstruction of Gene Regulatory Networks (ARACNe) algorithm was used to construct MSC-specific transcriptional interactome as described in our previous papers (16, 17). The Rattus norvegicus transcription factors (TFs) were collected from Animal Transcription Factor Database 3.0 (AnimalTFDB 3.0). From the combined microarray data of GSE87439, GSE15713, and GSE21573, a consensus gene network was generated by 100 rounds of ARACNe bootstrapping (http://califano.c2b2.columbia.edu/aracne/). MRA-Fisher's exact test (FET) was used to infer master regulator candidates and their transcriptional targets in A7r5 cell-specific transcriptional interactome. The ARACNe preprocessing and MRA-FET analysis were

run in geWorkbench software version 2.6.0 (http://wiki.c2b2.columbia.edu/workbench/index.php/Home)

Assessment of ligand - receptor interactions (CellPhoneDB).

We used CellPhoneDB (version 3.1.0; 18) to identify the potential ligand–receptor interactions for bone marrow MSC KO environment based on the raw count matrices. For WT and Hes1 KO groups, the means expression of interacting ligands in the sender population and interacting receptors in the receiver population were computed, and a one-sided Wilcoxon signed-rank test was used to assess the statistical significance of each interaction score.

ELISA

Whole bone marrow cells (WBMCs) from one femur were collected from the indicated mice 24h post 500 cGy TBI. After centrifugation, BM supernatants were collected into Isove's modified Dulbecco's medium (IMDM) and analyzed for TNF-α, CXCL4, IL-1β or CCL11 concentration using ELISA kit (Cat# MTA00B; MAB350; MLB00C and MME00; R&D systems) following the manufacturer's instruction.

Reporter gene assays

A total of 10^6 MSCs from *Hes1*-KO mice were transfected with a NFATc2 reporter construct containing 1.5 kB of the proximal NFATc2 promoter, pGL3-KB-Luc (NFAT Luciferase reporter (Addgene; 19) and plated on a 6-well plate. After 48 hours, cells were incubated with the indicated proteins (30 μg/mL). The cells were harvested 12 hours after treatment, washed with PBS, and luciferase activity was assessed using the dual luciferase assay reporter kit (Promega, Madison, WI).

Chromatin immunoprecipitation (ChIP)

ChIP assays were performed using a Magna ChIP A/G Chromatin Immunoprecipitation Kit (Millipore, Billerica, MA, USA; No. 17-10085) according to the protocol (20). Briefly, the cells were treated with 1% formaldehyde for 10 min at room temperature to cross-link DNA and proteins, and 125 mM glycine was used to quench residual formaldehyde for 5 min. After the wells were washed with cold PBS, they were lysed in lysis buffer for 15 min on ice. Then, crosslinked DNA in the lysates was sheared to fragments of 200 ~ 1000 base pairs (bp) by sonication (six times, 15 s each time with 50 s rest). The obtained samples were immunoprecipitated with anti-HES1 antibody (Novus Biologicals, Centennial, CO; NBP1-47791) or anti-IgG antibody (Cell Signalling Technology, Boston, MA, USA; No. 2729s) overnight at 4°C. Immunoprecipitated complexes were collected using Protein A/G magnetic beads. The complex was digested by proteinase K at 65°C for 2 h, and beads were separated by a magnetic device. Then, DNA fragments were purified and assessed by PCR and agarose gel electrophoresis. The sequences of primers used for PCR were synthesized by IDT and are listed in Supplementary Table S2. RNA extraction and quantitative real-time polymerase chain reaction (qRT-PCR; 21).

Statistical analysis

Paired or unpaired student's *t-test* was used for two-group comparisons. Survival data were plotted by the Kaplan-Meier curve method and analyzed by the log-rank test. Values of $p<0.05$ were considered statistically significant. Results are presented as mean ± SD. * indicates $p<0.05$; ** indicates $p<0.01$.

References:

1. Huang S, Xu L, Sun Y, et al. An improved protocol for isolation and culture of mesenchymal stem cells from mouse bone marrow. J Orthop Transl. 2015;3:26-33.
2. Delorme B, Ringe J, Gallay N, et al. Specific plasma membrane protein phenotype of culture-amplified and native human bone marrow mesenchymal stem cells. Blood. 2008;111:2631-2635.
3. Houlihan DD, Mabuchi Y, Morikawa S, et al. Isolation of mouse mesenchymal stem cells on the basis of expression of Sca-1 and PDGFR-a. Nat Protoc. 2012;7:2103-2111.
4. Wu X, Estwick SA, Chen S, et al. Neurofibromin plays a critical role in modulating osteoblast differentiation of mesenchymal stem/progenitor cells. Hum Mol Genet. 2006;15:2837-2845.
5. Zhang P, Xing C, Rhodes SD, et al. Loss of Asxl1 Alters Self-Renewal and Cell Fate of Bone Marrow Stromal Cells Leading to Bohring-Opitz-like Syndrome in Mice. Stem Cell Rep. 2016;6(6):914-925.
6. Zhang P, Chen Z, Li R, et al. Loss of ASXL1 in the bone marrow niche dysregulates hematopoietic stem and progenitor cell fates. Cell Discov. 2018;4:4.
7. Liao Y, Smyth GK, Shi W. The Subread aligner: fast, accurate and scalable read mapping by seed-and-vote. Nucleic Acids Res. 2013;41(10):e108-e108.
8. McCarthy DJ, Chen Y, Smyth GK. Differential expression analysis of multifactor RNA-Seq experiments with respect to biological variation. Nucleic Acids Res. 2012;40(10):4288-4297.
9. Ritchie ME, Phipson B, Wu D, et al. limma powers differential expression analyses for RNA-sequencing and microarray studies. Nucleic Acids Res. 2015;43(7):e47-e47.
10. Wagner GP, Kin K, Lynch VJ. Measurement of mRNA abundance using RNA-seq data: RPKM measure is inconsistent among samples. Theory Biosci. 2012;131(4):281-285.
11. Gu Z, Eils R, Schlesner M. Complex heatmaps reveal patterns and correlations in multidimensional genomic data. Bioinformatics. 2016;32(18):2847-2849.
12. Team RC. R: A Language and Environment for Statistical Computing. R Foundation for Statistical Computing, Vienna 2021. https://www.R-project.org.
13. Subramanian A, Tamayo P, Mootha VK, et al. Gene set enrichment analysis: a knowledge-based approach for interpreting genome-wide expression profiles. Proc Natl Acad Sci U S A. 2005;102(43):15545-15550.
14. Csardi MG: Package 'igraph'. Last accessed 2013;3(09):2013.
15. Lee S, Deng L, Wang Y, Wang K, Sartor MA, Wang X-S. IndepthPathway: an integrated tool for in-depth pathway enrichment analysis based on single-cell sequencing data. Bioinformatics. 2023;39(6):btad325.
16. Lee S, Chun JN, Kim SH, So I, Jeon JH. Icilin inhibits E2F1-mediated cell cycle regulatory programs in prostate cancer. Biochem Biophys Res Commun. 2013;441(4):1005-10
17. Lee S, Park YR, Kim SH, et al. Geraniol suppresses prostate cancer growth through down-regulation of E2F8. Cancer Med. 2016 Oct;5(10):2899-2908.

18. Efremova M, Vento-Tormo M, Teichmann SA, Vento-Tormo. R: CellPhoneDB: inferring cell-cell communication from combined expression of multi-subunit ligand-receptor complexes. Nat Protocols. 2020;15(4):1484-1506.
19. Ichida M, Finkel T. Ras regulates NFAT3 activity in cardiac myocytes. J Biol Chem. 2001. 276(5):3524-3530.
20. Wu L, Li X, Lin Q, Chowdhury F, Mazumder MH, Du W. FANCD2 and HES1 suppress inflammation-induced PPARɣ to prevent haematopoietic stem cell exhaustion. Br J Hematol. 2021;192(3):652-663
21. Sharma D, Mirando AJ, Leinroth A, Long JT, Karner CM, Hilton MJ. HES1 is a novel downstream modifier of the SHH-GLI3 axis in the development of preaxial polydactyly. PloS Genet. 2021;17(12):e1009982.

Supplementary tables

Table S1. Steady state hematological parameter of *Hes1$^{fl/fl}$Prx1Cre* mice.

	Absolute and differential WBC counts				Characterization of red blood cells				Plts
	WBC(cells/ul)	Lymphocyte (%)	Neutrophils (%)	Monocytes (%)	RBC (X10^{12}/L)	HCT (%)	MCV (fL)	Hb (g/dL)	(X10^{9}/L)
Hes1$^{fl/fl}$	7.15±2.24	61.2±8.5	27.1±14	3.82±2.1	8.16±1.13	43.8±6.71	53.91±1.72	12.49±1.5	608.1±187
Hes1-KO	8.732±3.41	61.08±21	34.17±21	4.945±1	8.71±1.72	44.93±8.05	52.08±3.18	12.93±2.7	761.2±240
P	0.5673	0.2615	0.5263	0.3531	0.413	0.718	0.4044	0.615	0.26961

Table S2. qPCR primers

	Primers used for qPCR	
Gene	Forward	Reverse
Hes1	GGAAATGACTGTGAAGCACCTCC	GAAGCGGGTCACCTCGTTCATG
Nfatc2	ACTTCACAGCGGAGTCCAAGGT	GGATGTGCTTGTTCCGATACTCG
Tnfa	GGTGCCTATGTCTCAGCCTCTT	GCCATAGAACTGATGAGAGGGAG
Cxcl4	GTTGTTTCTGCCAGCGGTGGTT	ACAGTGGCGTCCTGCCTTGATC
Il1b	TGGACCTTCCAGGATGAGGACA	GTTCATCTCGGAGCCTGTAGTG
Ccl11	TCCATCCCAACTTCCTGCTGCT	CTCTTTGCCCAACCTGGTCTTG
Gapdh	TCAATGAAGGGGTCGTTGAT	CGTCCCGTAGACAAAATGGT
	Primers used for ChIP assay	
Gene	Forward	Reverse
N Class E box	TGGGAAGTTTCACACGAGCC	ATCTGCCATTTCACCCCGAG
B class E box	TCCGTCAGCCGGAAGTACAG	CAACTTCTGCTTCACCTGCT

Supplementary figures

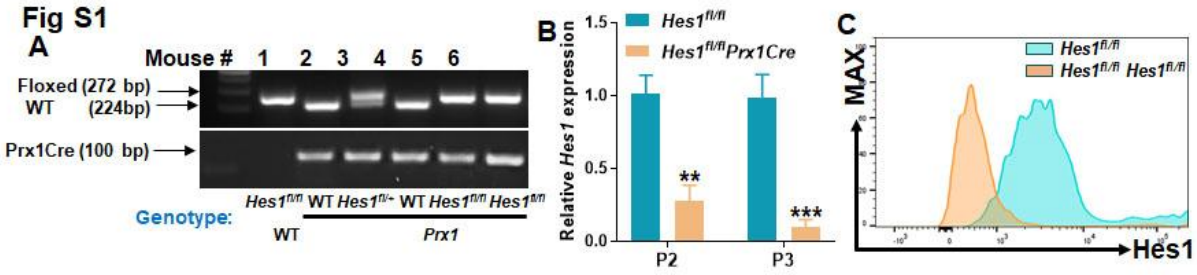

Fig S1. Validation of MSC specific *Hes1* deletion. A. Genotyping of *Hes1*$^{fl/fl}$*Prx1Cre* mice and their *Hes1*$^{fl/fl}$ littermates. Genomic DNA was extracted from tails collected from *Hes1*$^{fl/fl}$*Prx1Cre* mice and their *Hes1*$^{fl/fl}$ littermates followed by PCR reaction. DNA gel image indicates expected PCR products for WT allele (224bp) and floxed allele (272 bp). B. qPCR verifies *Hes1* deletion in MSCs. RNA was extracted from MSCs (Passage 2, Left; Passage 3, Right) isolated from *Hes1*$^{fl/fl}$*Prx1Cre* mice and their *Hes1*$^{fl/fl}$ littermates followed by qPCR analysis for *Hes1*. Samples were normalized to the level of *GAPDH* mRNA. C. Intercellular Hes1 staining. MSCs from *Hes1*$^{fl/fl}$*Prx1Cre* mice and their *Hes1*$^{fl/fl}$ littermates were subjected to intracellular Hes1 staining after passaged twice in *ex vivo* culture.

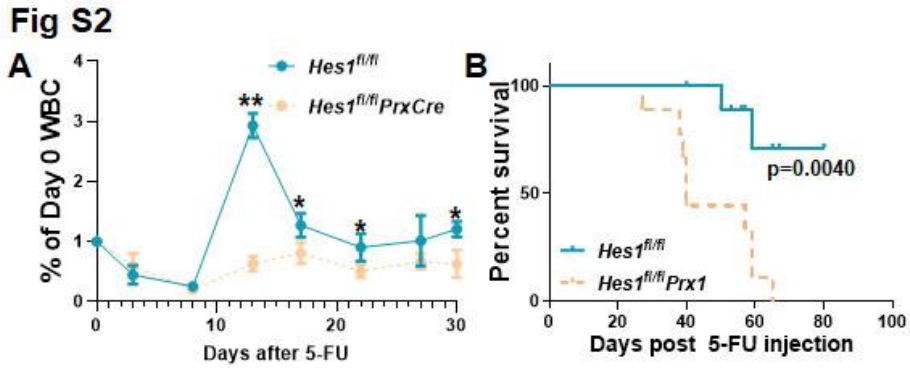

Fig S2. *Hes1*$^{fl/fl}$*Prx1Cre* mice are hypersensitive to 5-FU challenge. A. *Hes1*$^{fl/fl}$*Prx1Cre* mice exhibit lagging recovery kinetics after 5-FU injection. The white blood cell (WBC)

count of *Hes1*$^{fl/fl}$ and *Hes1*$^{fl/fl}$*Prx1Cre* mice after a single injection of 5-FU (150 mg/kg) was monitored over time. B. *Hes1*$^{fl/fl}$*Prx1Cre* mice are hypersensitive to 5-FU treatment. 5-FU (135 mg/kg) was administrated to *Hes1*$^{fl/fl}$*Prx1Cre* mice and their *Hes1*$^{fl/fl}$ and *Hes1*$^{fl/fl}$ littermates weekly for 3 consecutive weeks. Survival of the animals was plotted by the Kaplan-Meier curve method and analyzed by the log-rank test.

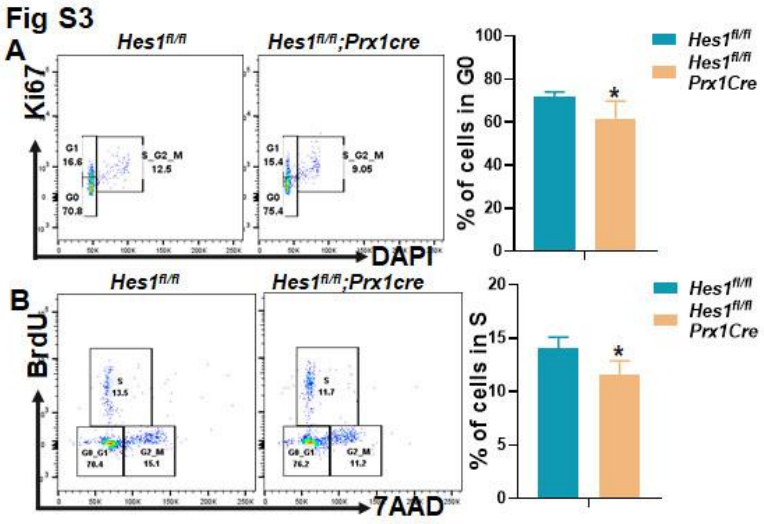

Fig S3. MSCs from *Hes1*$^{fl/fl}$*Prx1Cre* mice are more quiescent. WBMCs from *Hes1*$^{fl/fl}$*Prx1Cre* and *Hes1*$^{fl/fl}$ mice were subjected to flow cytometry analysis for ki67 and DAPI (A) and BrdU incorporation (B). Representative flow plot (Left) and quantification (Right) are shown.

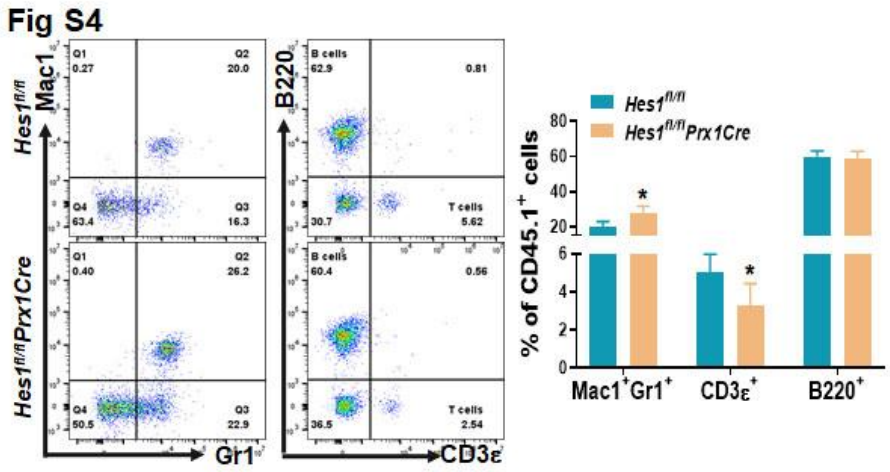

Fig S4. Lineage differentiation in BMT recipients. WBMCs from BoyJ mice (CD45.1$^+$) were transplanted into lethally irradiated *Hes1$^{fl/fl}$Prx1Cre* and *Hes1$^{fl/fl}$* mice. Lineage differentiation in *Hes1$^{fl/fl}$Prx1Cre* recipients. PB from the recipient mice described in B were subjected to flow cytometry for CD3ε/B220, Gr1/Mac1.

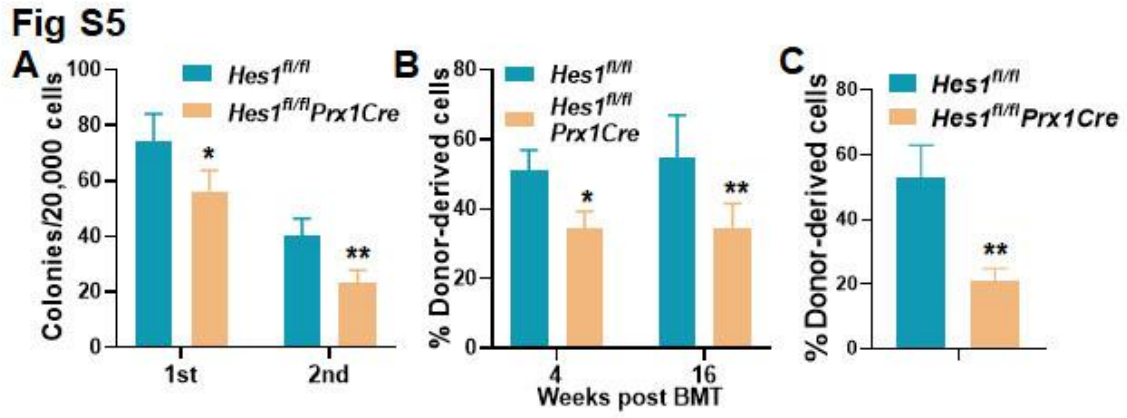

Fig S5. HSPCs from *Hes1$^{fl/fl}$Prx1Cre* mice are functionally defective. A. Loss of *Hes1* in BM niche affects HSPC progenitor activity. WBMCs from *Hes1$^{fl/fl}$Prx1Cre* or *Hes1$^{fl/fl}$* mice were plated in cytokine-supplemented methylcellulose medium. Colonies were enumerated on day 7. Results are means ±standard deviation (SD) of three independent experiments (n = 6~9 per group). B. Mesenchymal *Hes1* deletion compromises

hematopoietic reconstitution in the recipients. WBMCs, along with $2X10^5$ competitor cells from congenic BoyJ mice were transplanted into lethally irradiated BoyJ recipients. Donor-derived chimera was detected 16 weeks post BMT. C. *Hes1* deletion impair long-term reconstitution. WBMCs from the primary recipients described in B were transplanted into sublethally irradiated BoyJ recipients. 2^{nd} BMT. Donor-derived chimera was detected 16 weeks post BMT.

Supplementary Figure 6

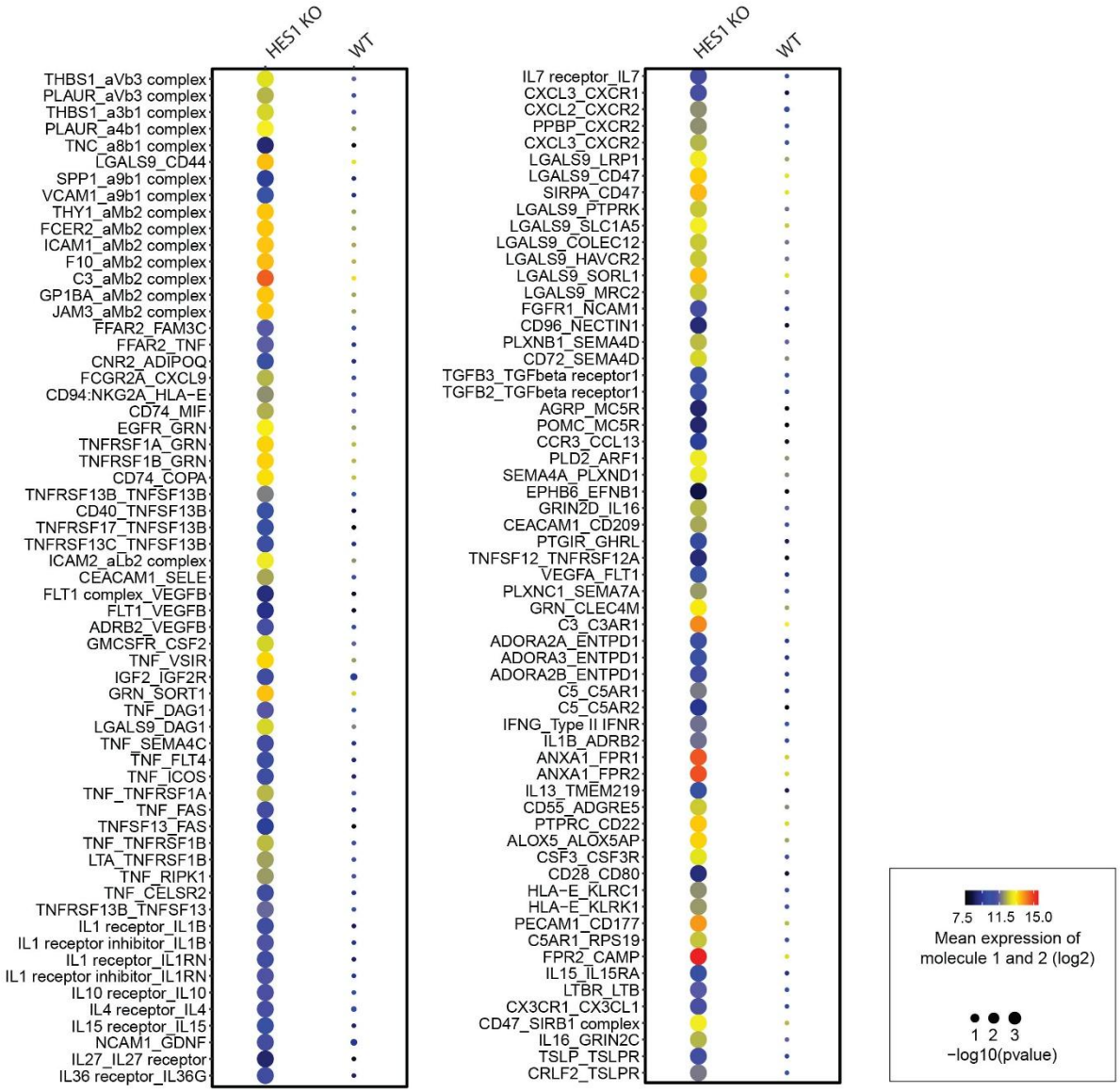

Fig S6. Inflammation panel. CellPhoneDB analysis was conducted to identify gene pairs of ligand-receptor expressed in the BM cells using the RNA-seq data described in Fig 5. Using CellPhoneDB pipeline, statistically significant mean expression of ligand-receptor genes was determined in *Hes1*-KO or control group. Size indicates -log10(*p*-values), and color indicates the mean expression of the ligand-receptor pairs in individual groups.

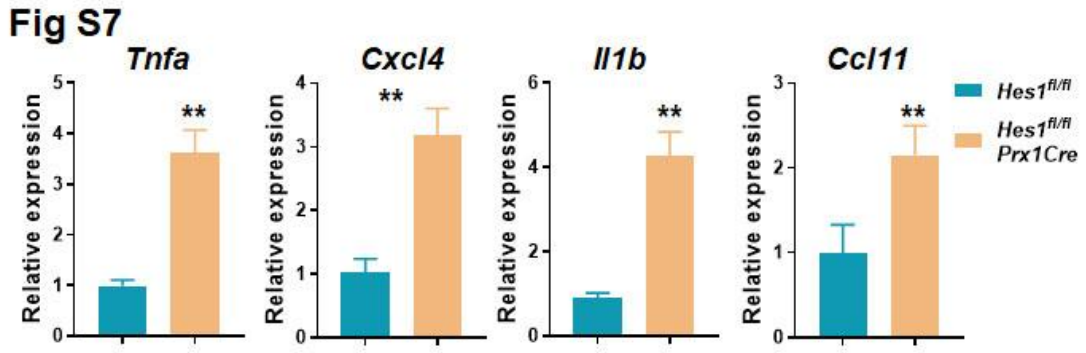

Fig S7. qPCR analysis of inflammatory genes identified from transcriptomics analysis. RNA extracted from MSCs, isolated from *Hes1*$^{fl/fl}$*Prx1Cre* mice and their *Hes1*$^{fl/fl}$ littermates were subjected to quantitative RT-PCR using primers listed in Table S2. Samples were normalized to the level of *GAPDH* mRNA.

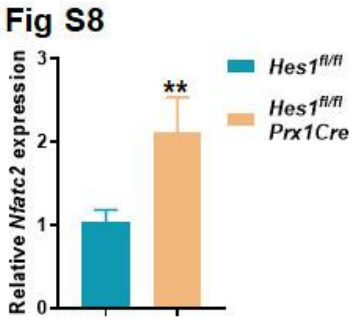

Fig S8. Reduced NFATc2 in *Hes1*-KO MSCs. RNA was extracted from MSCs (Passage 2) isolated from *Hes1*$^{fl/fl}$*Prx1Cre* mice and their *Hes1*$^{fl/fl}$ littermates followed by qPCR analysis for *Nfatc2*. Samples were normalized to the level of *GAPDH* mRNA.